1-1-2006

Use of neutron diffraction and microscopy for characterization of residual stresses and defects

Silpa Budugur Suresh
University of Nevada, Las Vegas

USE OF NEUTRON DIFFRACTION AND MICROSCOPY FOR CHARACTERIZATION OF RESIDUAL STRESSES AND DEFECTS

by

Silpa Budugur Suresh

Bachelor of Science in Mechanical Engineering
Sri Venkateswara University, India
June 2003

A thesis submitted in partial fulfillment
of the requirements for the

Master of Science in Mechanical Engineering
Department of Mechanical Engineering
Howard R.Hughes College of Engineering

Graduate College
University of Nevada, Las Vegas
December 2005

UNLV
UNIVERSITY OF NEVADA LAS VEGAS

Thesis Approval
The Graduate College
University of Nevada, Las Vegas

November 17, 20 05

The Thesis prepared by

Silpa Budugur Suresh

Entitled

Use of Neutron Diffraction and Microscopy for Characterization of Residual Stresses and Defects

is approved in partial fulfillment of the requirements for the degree of

Master of Science in Mechanical Engineering

Examination Committee Chair

Dean of the Graduate College

Examination Committee Member

Examination Committee Member

Graduate College Faculty Representative

1017-53

ABSTRACT

Use of Neutron Diffraction and Microscopy for the Characterization of Residual Stress and Defects

by

Silpa Budugur Suresh

Dr. Ajit K. Roy, Examination Committee Chair
Associate Professor of Mechanical Engineering
University of Nevada, Las Vegas

The structural material to contain the target material, used in transmutation of spent nuclear fuel, may develop residual stress due to different forming processes. Nondestructive neutron diffraction (ND) and positron annihilation spectroscopy (PAS) techniques have been utilized to characterize residual stress in martensitic Alloys EP-823 and HT-9, subjected to cold-reduction, plastic deformation and welding. The ND measurements revealed tensile residual stresses on the top and bottom surfaces of the cold-worked specimens. The residual stress was enhanced in cylindrical specimens with increased plastic-deformation. Post-weld-thermal-treatment was benificial to reduce internal stresses in welded specimens. The line-shape-parameters (S, W and T) obtained from the PAS spectrum were related to the residual stress developed in cold-worked and plastically deformed specimens. The dislocation density determined by transmission electron microscopy was enhanced at higher cold-reduction levels. Fractographic evaluations by scanning electron microscopy revealed ductile failures in cylindrical specimens.

TABLE OF CONTENTS

LIST OF FIGURES

ACKNOWLEDGEMENTS

Greatest acknowledgement to my advisor, Dr. Ajit K. Roy who guided, supported and constantly helped me in clarifying my doubts patiently through out my research.

I would like to thank Dr. Anthony Hechanova, Dr. Edward. S. Neumann and Dr. Woosoon Yim for their valuable suggestions. I would like to thankfully acknowledge the guidance of Dr. Ron Donaberger and Dr.Ron Rogge at AECL, Dr. Douglas Wells at ISU and Dr. Longzou Ma at UNLV.

I would like to acknowledge with appreciation the moral support provided by my friends Prerna and Aparna. Help extended by each member of the Materials Performance Laboratory and my colleague Subhra is truly acknowledged.

I would like to acknowledge the US Department of Energy for the financial support for my research included in this thesis.

CHAPTER 1

INTRODUCTION

The disposal of spent-nuclear-fuel (SNF) and high-level radioactive waste (HLW) is a major challenge to nuclear power generating nations. In order to circumvent the problems associated with the nuclear waste disposal, the United States Department of Energy (USDOE) has been considering the development of a permanent geologic repository at the yucca mountain site, located 100 miles northwest of Las Vegas, Nevada. [1] Even though, the proposed repository is being developed to accommodate a substantial amount of SNF/HLW, additional nuclear waste is gradually being generated in the United States from the current operating nuclear power plants. Therefore, development of more repositories may be needed in the near future to accommodate the nuclear waste currently being generated.

While the geologic repository at the yucca mountain site is being designed, the USDOE is considering a new concept to reduce the radioactivity of SNF/HLW by a process known as transmutation. Transmutation refers to the transformation of SNF and occurs when the nucleus of an atom changes due to the natural radioactive decay, nuclear fission, neutron capture or other related processes. This process enables the transformation of long-lived isotopes to species with relatively short half-lives and reduced radioactivity through capture and decay of minor actinides and fission products.

[2] Thus, this process may enable geologic disposal of SNF for shorter durations in the proposed yucca mountain repository, enhancing the disposal efficiency.

The molten lead-bismuth-eutectic (LBE) has been proposed to be a spallation target producing source neutrons from the incident photon beams from an accelerator or a reactor and simultaneously acting as a blanket coolant, thus removing the generated heat. The operating concept [3] for transmutation is illustrated in Figure 1.1

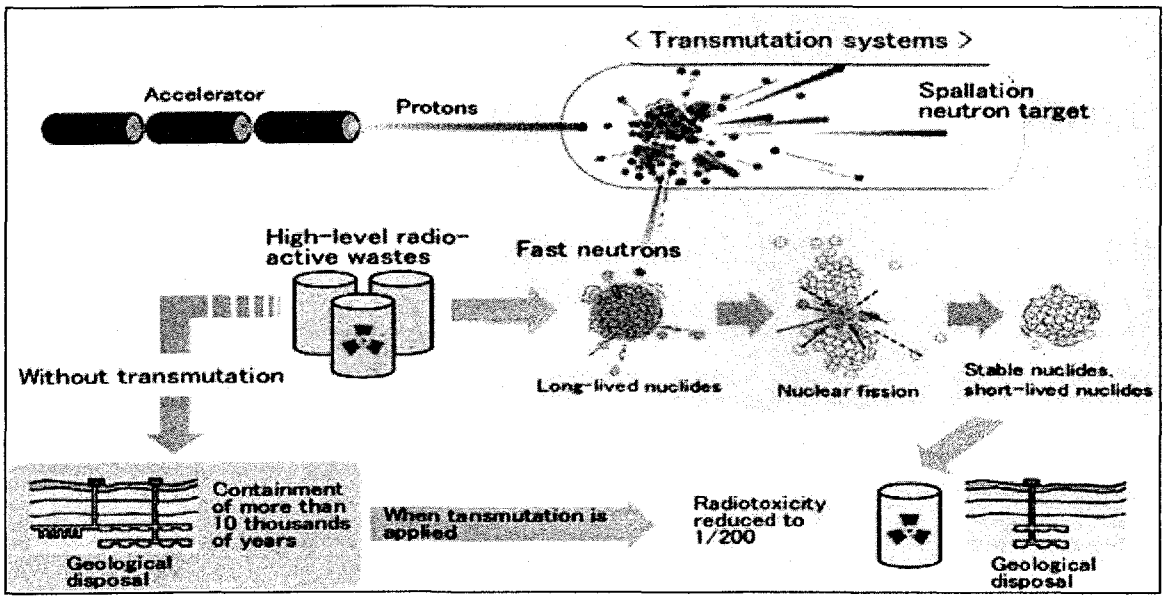

Figure 1.1 Concept of Transmutation

The molten LBE will be contained in a structural vessel made of suitable metallic materials, often referred to as target structural materials. Fabrication of this containment vessel will involve normal manufacturing processes such as cold-deformation, mechanical forming, and welding of similar and dissimilar materials. A significant amount of residual stress can be developed in the container materials during the

fabrication process unless they are minimized or eliminated by stress-relief operations. However, stress-relief or annealing treatment at elevated temperatures may not be feasible in view of the possible changes in metallurgical characteristics of these structural materials, producing detrimental effects during the spallation process.

Welding operations involving either similar or disimilar structural material can lead to the development of internal stresses resulting from rapid rate of solidification, differences in thermal coefficient of expansion/contraction, and disimilar metallurgical microstructures developed at the weld, fusion line, heat-affected-zone (HAZ) and the base metal. Combination of these residual stresses and the elevated temperatures used during the transmutation process can adversely influence the performance of the target structural material.

Residual or internal stresses are usually defined as stresses remaining in a material or a body following its manufacturing and processing in the absence of external forces or thermal gradients. Any manufacturing processes that involve forging, rolling, and bending at elevated temperatures can induce this type of internal stress. The residual stresses, which are usually three dimensional, can be either macro or micro-stresses, which can contribute to premature failures due to fatigue, stress-corrosion, and corrosion fatigue, and hydrogen embrittlement.

Residual stresses can be divided into three types. The first type of stress may vary over a large scale comparable to the macroscopic dimensions of structural components, and are referred to as macro-stresses. This type of stress can extend through a part over longer distances typically a few thousandths of a meter or a millimeter. They are present in weldments and joined components of similar and disimilar materials, which can be

spatially resolved or mapped. Different types of stresses are shown in Figure 2. The second type of stress can vary over a smaller range comparable to the grain size and can, for example, be related to the differences in mechanical and thermal properties of structural components in multi-phase materials. [4] This type of stress is commonly called the micro-stress. The development of micro-stress can occur across distances approaching a few millionths of a meter or a micrometer, which can cause failure of parts during manufacturing as well as under static and dynamic loading. Finally, these type of stresses, which are quite insignificant from the failure point of view can vary within each individual grains.

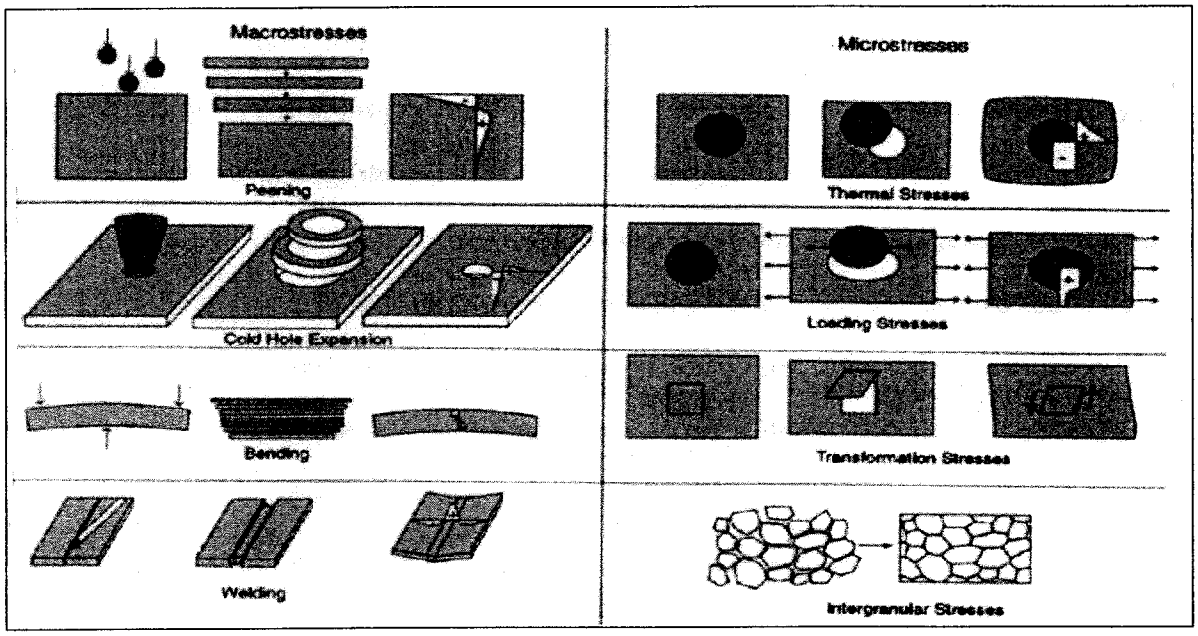

Figure 1.2 Different types of macro and micro residual stresses

Residual stress can be either tensile or compressive depending on the material and the manufacturing processes imparted to them. Both the magnitude and the distribution of

residual stress may be critical to the performance and should, therefore, be considered in the design of a component. The tensile residual stresses are detrimental, increasing the susceptibility of a material to fatigue damage, stress-corrosion and fracture. On the contrary, the compressive residual stresses are benificial, thus, reducing the material's susceptibility to failure. [5] Nevertheless, residual stresses of either type can adversely influence the dimensional stability of a component. An equilibrium must be maintained between the tensile and a compressive residual stresses existing within a component for optimum level of performance.

While many different techniques are commercially available to characterize the residual stresses in components subjected to plastic deformation, cold-reduction and welding, significant efforts have been made in this investigation to use the nondestructive methods. These techniques include neutron diffraction (ND) and positron annihilation spectroscopy (PAS). However, a major emphasis has been placed on ND in this investigation to characterize the resultant residual stresses in all three types of specimens. The ND technique can provide complete three-dimensional strain maps achieved by translational and rotational movements of the component. It employs the low velocity thermal neutrons to measure the lattice spacing (d-spacing) between consecutive crystallographic planes that helps in the measurement of strains by the use of Bragg's law. The magnitude of the internal stresses corresponding to these strains can be calculated using the elastic constants of a material of interest.

Two methods based on the conventional PAS technique have been used in this study. They are pair-production and activation methods. Both methods provide a qualitative characterization of residual stress in terms of line-shape parameters determined from the

associated energy spectrum. The residual stress measurements of the tested specimens by pair-production and the activation methods were performed at the Idaho Accelerator Center of the Idaho State University. The ND measurements were performed at the Atomic Energy of Canada Limited, Chalk River laboratory.

Attempts have been made in this study to analyze the resultant residual stress data involving cold-worked, plastically deformed and welded structural materials such as martensitic Alloy EP-823 and Alloy HT-9. Since the residual stresses generated in the welded specimens can be minimized by post-weld-thermal-treatment (PWTT), the welded specimens have been analyzed with and without PWTT using the ND method. Different levels of plastic-deformation and reduction in thickness were given to the test materials prior to the characterization of the resultant internal stresses. The metallographic evaluations of the tested specimens were performed by optical microscopy. The fractrographic evaluations of specimens subjected to plastic deformation by tensile loading were conducted by scanning electron microscopy (SEM). The characterization of defects such as dislocations and their densities in the cold-worked materials was performed by transmission electron microscopy (TEM). The overall data including residual stress characterization and microscopic evaluations are presented in this thesis.

CHAPTER 2

TEST MATERIALS AND SPECIMENS PREPARATION

2.1 Test Materials

Several factors need to be considered to select the structural material for transmutation applications. These factors include mechanical, thermal, physical and chemical properties, cost, availability, capability of withstanding radiation damage and some neutronic factors. Martensitic steels have been widely used as structural materials in many reactor facilities. The primary advantages of martensitic steels are their high resistance to void swelling, low irradiation creep rates and relatively low radioactivation after neutron irradiation.

Martensitic stainless steels (SS) are essentially alloys of chromium and carbon that possess a body-centered-cubic (bcc) or body-centered-tetragonal (bct) crystal structure in the hardened condition. They are ferromagnetic and hardenable by heat treatments. [6] Their general resistance to corrosion is adequate for some corrosive environments, but not as good as other stainless steels. Higher carbon (C) contents will produce greater hardness and, therefore, may lead to the increased susceptibility to cracking. The chromium (Cr) content of these materials generally ranges from 9 to 18 weight percent (wt %), and the carbon content can be as high as 1.2 wt %. Molybdenum (Mo) and nickel (Ni) can be added to improve the mechanical properties and the

corrosion resistance. [7] The test materials used in this investigation include martensitic Alloy EP-823 and Alloy HT-9.

Fe-Ni-Cr-Mo and a primary candidate material for use as cladding in the current U.S. fast Alloy EP-823 is a Russian nuclear grade martensitic iron-nickel-chromium molybdenum (Fe-Ni-Cr-Mo) SS with a high silicon (Si) content (1.0-1.3 wt %). It is a leading structural material to contain the molten LBE nuclear coolant needed for fast spectrum operations of the ADS systems. This alloy has also been reported to retain its high strength and ductility at elevated temperatures in irradiated conditions.[8] At 500°C, this Alloy exhibits high strength and when irradiated it can retain high post-irradiation ductility at test temperatures in the range of 20-700°C.

Alloy HT-9 is a Swedish nuclear grade martensitic reactor designs. [9] Alloy HT-9 was specifically developed for high temperature applications, where the corrosion-resistance inherent in austenitic stainless steels is not required. It has good swelling resistance and is also resistant to irradiation embrittlement particularly at 60°C. [10] It has been an excellent material for duct applications in liquid-metal reactors. Moderate strength, ample corrosion resistance, and excellent resistance to swelling in the fast neutron environment have made Alloy HT-9 a primary candidate material for use in many nuclear applications. The typical physical and mechanical properties of these two materials are given in Table 2.1. [11, 12]

Experimental heats of both test materials were melted by a vacuum-induction-melting practice at the Timken Research Laboratory, Canton, OH, followed by

different fabricating processes that included forging and hot rolling. Since significant amount of residual or internal stresses were generated during these manufacturing processes, the test materials were subsequently thermally-treated to relieve these internal stresses, and achieve the desired metallurgical microstructures. These thermal treatments included austenitizing at 1850°F followed by an oil-quench subsequently, they were tempered at 1150°F followed by air-cooling. These types of thermal-treatments resulted in a fully-tempered and fine-grained microstructure characteristics of a martensitic stainless steel without the formation of any retained austenite. The chemical compositions of both heats are shown in Table 2.2.

Table 2.1 Physical and Mechanical Properties of the Materials Tested

Property	**Alloy EP-823**	**Alloy HT-9**
Thermal Conductivity(W/m*K)	NA	28
Modulus of Elasticity, Gpa (10 psi)	207	160
Poisson's Ratio at Ambient Temperature	0.29	0.33
Coefficient of thermal Expansion C * 10	NA	12.5

NA- Not Available

Table 2.2 Chemical Composition of Materials Tested (wt %)

Elements	Material/Heat No.	
	Alloy EP-823/2360	Alloy HT-9/2361
C	0.15	0.20
Mn	0.56	0.40
P	0.005	0.004
S	0.003	0.004
Si	1.21	0.18
Cr	11.81	12.32
Ni	0.67	0.49
Mo	0.73	0.98
Cu	0.01	0.01
V	0.32	0.29
W	0.63	0.43
Cb	0.27	-
B	0.0068	-
Ce	0.067	-
Al	0.033	0.025
Fe	Bal	Bal

Bal-Balance

2.2. Test Specimens

Three different types of test specimens were fabricated from the experimental heats. They include plastically-deformed and cylindrical specimens, and welded specimens consisting of similar and disimilar materials. Smooth cylindrical tensile specimens were machined from the heat-treated plates, in such a way that the gage section was parallel to the longitudinal rolling direction. The gage length to the diameter (l/d) ratio of these specimens was maintained at 4 according to the ASTM Designation E 8. [13] An axial/ tensional servo-hydraulic and computer controlled MTS unit was used to determine the tensile properties of both alloys at ambient temperature. The MTS test setup is shown in

the Figure 2.1 and the configuration of the smooth cylindrical specimen is shown in Figure 2.2. The heat-treated plate materials were subjected to cold-rolling to reduce their thickness by approximately 5 and 10 percent. Efforts were made to compare the residual stress in these cold-reduced plates with that of plates without any cold-reduction. The pictorial view and the dimensions of the cold-rolled plates are illustrated in Figure 2.2.

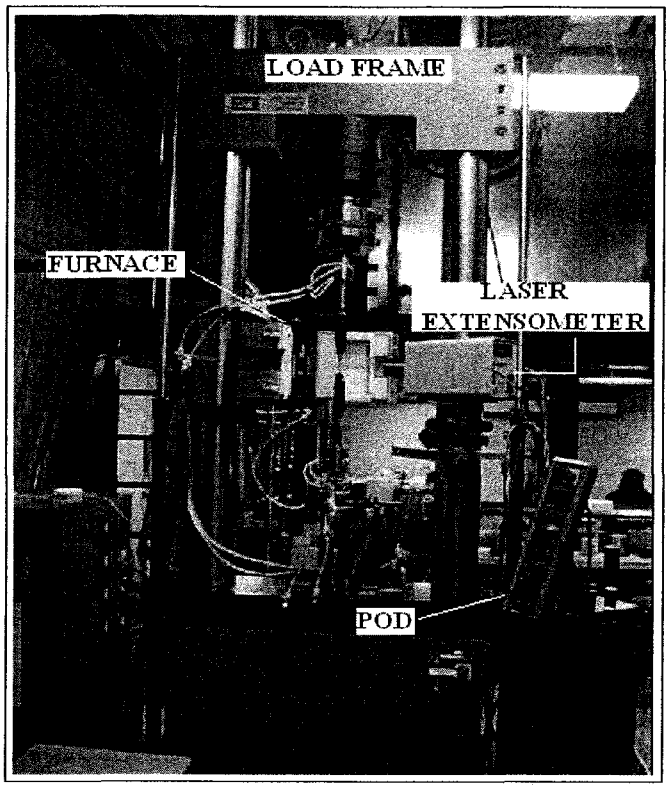

Figure 2.1 MTS Test Setup

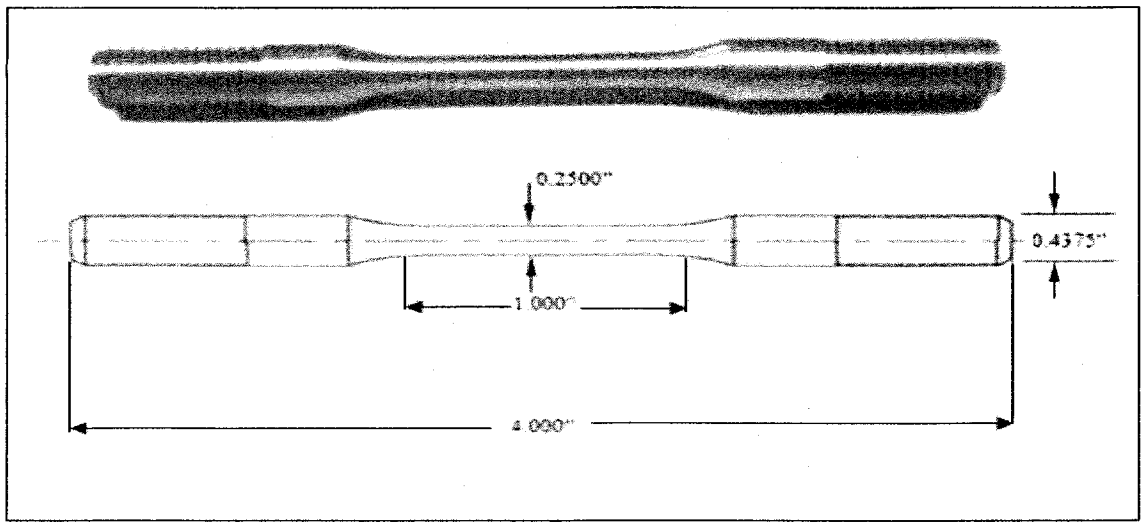

Figure 2.2 Configuration of the Cylindrical Specimen

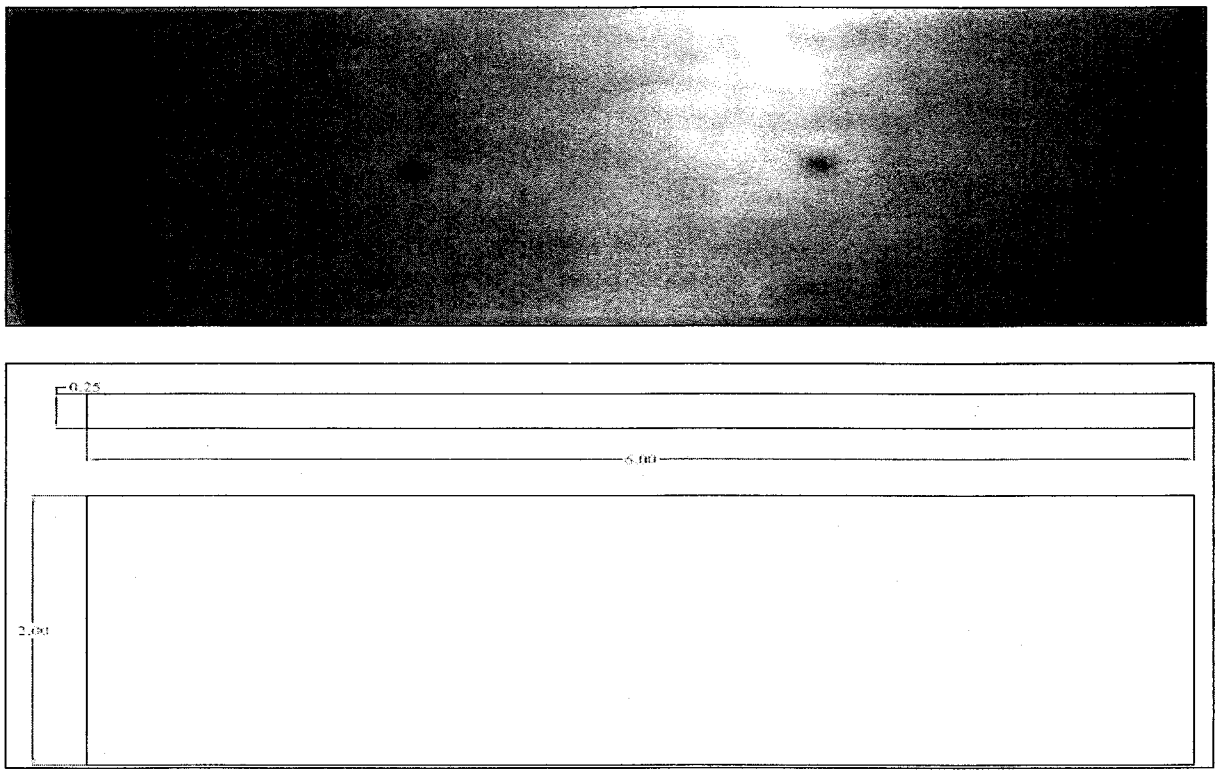

Figure 2.3 Configuration of the Cold-Worked Specimen

Martensitic steels are known to be the most difficult alloys to be welded. The configuration of the welded specimen is shown in the Figure 2.3. They are generally welded by gas-tungsten-arc-welding (GTAW). This process is widely used for thinner sections of stainless steel. The 2% tungsten is recommended and the electrode should be ground to a taper. [14] Argon is normally used for gas shielding, however, argon-helium mixtures are sometimes used for automatic applications. Welded specimens consisting of similar (Alloy HT-9 on both sides) and disimilar materials (Alloy HT-9 and Alloy EP-823) were prepared by GTAW process. The specimens were welded at the Apeks LLC

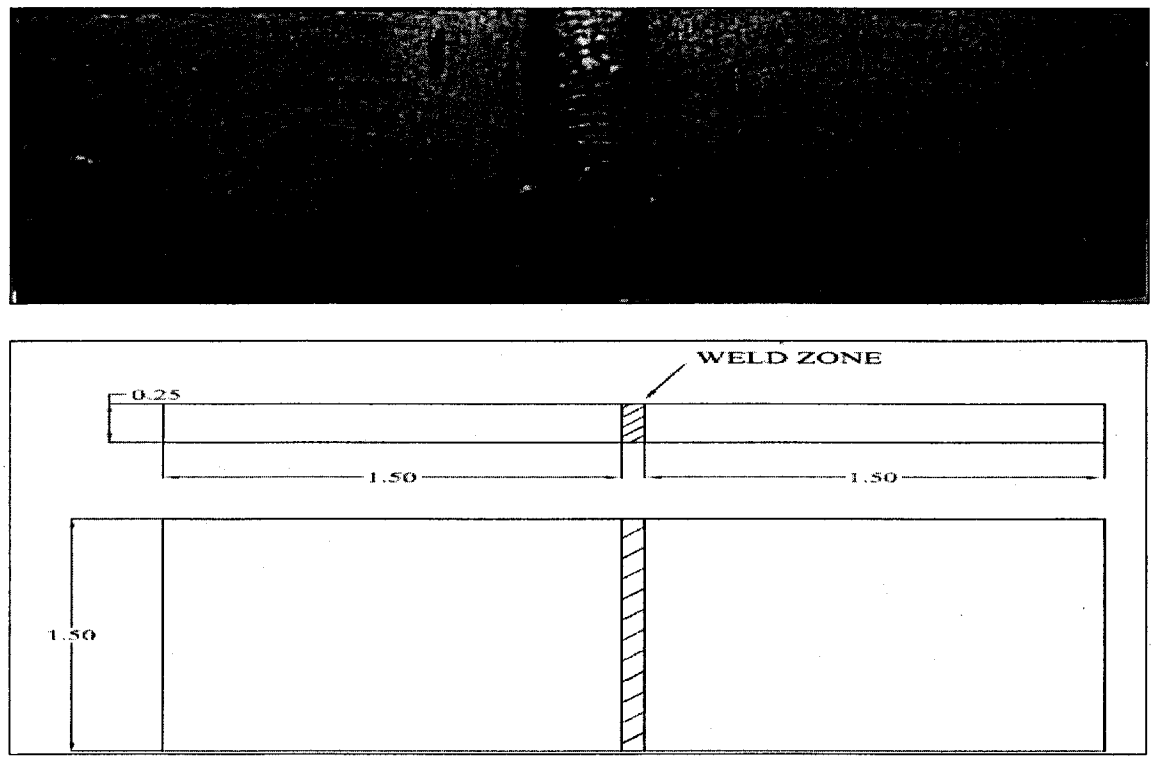

Figure 2.4 Configuration of the Welded Specimen

located at Ohio. The welded specimens were subjected to PWTT to eliminate or minimize the residual stresses generated during welding. Type 2283 L SS was used as a filler material for welding operation involving either alloy. [15] PWTT was done by heating at 1350-1400°F followed by controlled air cooling to 1100°F at a rate of 50 degrees per hour.

Characterization of metallurgical microstructures of the specimens by optical microscopy is important. Both the tensile and the welded specimens were sectioned properly and mounted in an epoxy resin by standard metallographic techniques. The polished and etched specimens were rinsed in deionized water, and dried with acetone and alcohol prior to their evaluation by a Leica optical microscope.

The fractrographic evaluation of the tested cylindrical specimen was performed by using a JEOL-5600 scanning electron microscope (SEM). This SEM was capable of resolution up to 100,000 times. TEM was used to characterize defects such as dislocations resulting from different levels of cold-reduction. The TEM sample thickness can vary from 100-200 microns, and the sample preparation involved many steps as described below.

The cold-worked plate material of Alloy EP-823 was initially cut in a transverse direction followed by a sectioning in the longitudinal direction. The longitudinally-cut piece was then subjected to a fine-cut by a diamond saw. The thickness of the small specimen ranged between 500 and 700 microns. This specimen was then mounted on a sample holder placed on a heater having an adjustable thermostat. Wax was placed on the specimens, which was melted causing binding of the specimen to the specimen holder which was then placed on a cold plate for cooling. The specimen holder is put into a

planar specimen grinder and the polishing was conducted on a rotary grinding/ polishing wheel. An abrasive 600 grit paper was used for mechanical polishing. [16] The thickness of the sample after mechanical polishing can be measured by a digital gage. The very thin specimens are then subjected to punching operation by punching an approximate 3-mm diameter hole by means of a punching tool. The punched specimens were then subjected to electro polishing producing a smooth specimen surface. The specimens were electropolished at 40 volts and at a flow rate of 12 at a temperature of -7°C (-19.4°F) using a solution of 5% perchloric acid in ethanol as an electrolyte.[17] Finally the specimens were cleaned with acetone and ethyl alcohol and the specimens were examined by TEM.

CHAPTER 3

EXPERIMENTAL TECHNIQUES

The characterization of residual stresses in candidate target structural materials, namely alloys EP-823 and HT-9, subjected to plastic deformation, cold-reduction, and welding, was performed by two nondestructive techniques. These techniques include positron annihilation spectroscopy (PAS) and neutron diffraction. (ND). The tested specimens were also evaluated by optical microscopy to determine their metallurgical microstructures. Transmission electron microscopy (TEM) was used to characterize the dislocation and determine the dislocation density from the TEM micrographs of the cold-worked specimens. The morphology of failure of cylindrical specimens used in calibration of tensile specimens was determined by scanning electron microscopy (SEM).

3.1 Calibration Curve Developments

Residual stress characterization by the positron annihilation spectroscopy (PAS) leads to qualitative information giving parameters derived from annihilation peaks. Therefore, the precise estimation of residual stress using these parameters is quite challenging. In order to provide a better estimation of residual stress in structural materials such as martensitic alloys EP-823 and HT-9, the development of calibration curves based on engineering stress vs. strain (s-e) diagrams was attempted using the ASTM designation

E8. The s-e diagrams for both the Alloys resulted in the identification of the yield strength (YS), ultimate tensile strength (UTS) and the failure stress (FS). The difference in the YS and UTS was recorded and the difference in stress magnitude in this range was divided in desired increments. The new cylindrical specimens were then loaded at these stress levels, and the corresponding strain values were recorded. These plastically deformed specimens were then subjected to residual stress characterization by nondestructive techniques including PAS and ND. The PAS technique was used for residual stress characterization of both Alloy EP-823 and Alloy HT-9. However the residual stress measurements by ND were performed only on plastically deformed Alloy EP-823.

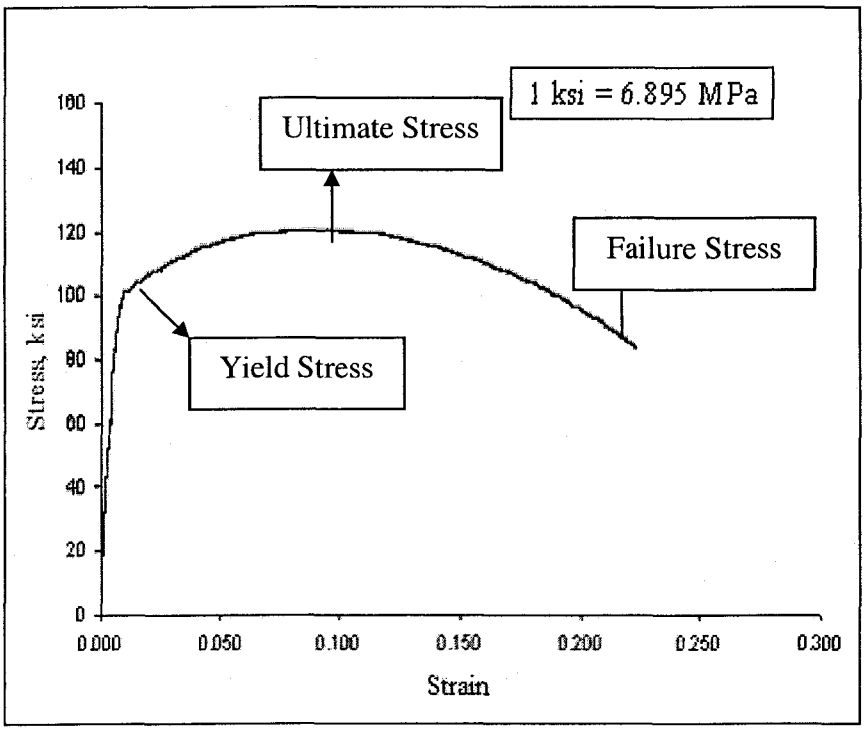

Figure 3.1 – Ambient-Temperature s-e Diagram for Alloy EP-823

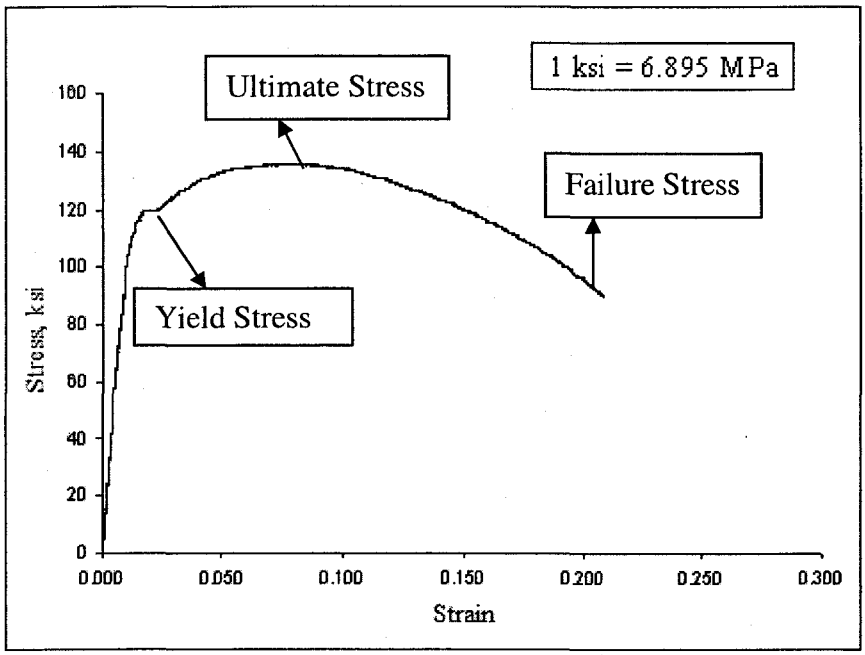

Figure 3.2 – Ambient-Temperature s-e Diagram for Alloy HT-9

EP-823. The extent of residual stress characterized by either technique was then related to the magnitude of stress/strain corresponding to the plastic deformation imparted to the cylindrical specimens by tensile loading. The s-e diagrams for Alloy EP-823 and Alloy HT-9 are shown in Figures 3.1 and 3.2, respectively.

3.2 Positron Annihilation Spectroscopy

For every matter particle, there is a corresponding anti-particle. Positron is the anti particle of an electron. It has the same mass of an electron but has an opposite charge.[18] PAS is a well-established nondestructive technique to characterize defects in metals and alloys. [19] Two different methods based on PAS, namely pair-production and activation have been used in this investigation to generate positrons. Both methods are known to be

capable of characterizing defects in thick specimens that cannot be evaluated by conventional positron technique or other nondestructive methods.

3.2.1 Pair-Production

This technique employed high-energy, deep penetrating γ-rays into thick samples of both materials of interest to measure stress, strain, and defects in them. A collimated photon beam from a linear accelerator (LINAC) was used to generate positrons inside the test specimen via pair (positron/electron) production, as shown in Figure 3.2. [20] Positron annihilation is a result of an encounter of the electron with its antiparticle - positron. The energy released by the annihilation forms two high energetic gamma photons, which travel in opposite direction. Thus, each positron generated was thermalized and annihilated with one of the sample electrons emitting two photons having 511 keV energy spectrum. [21, 22]

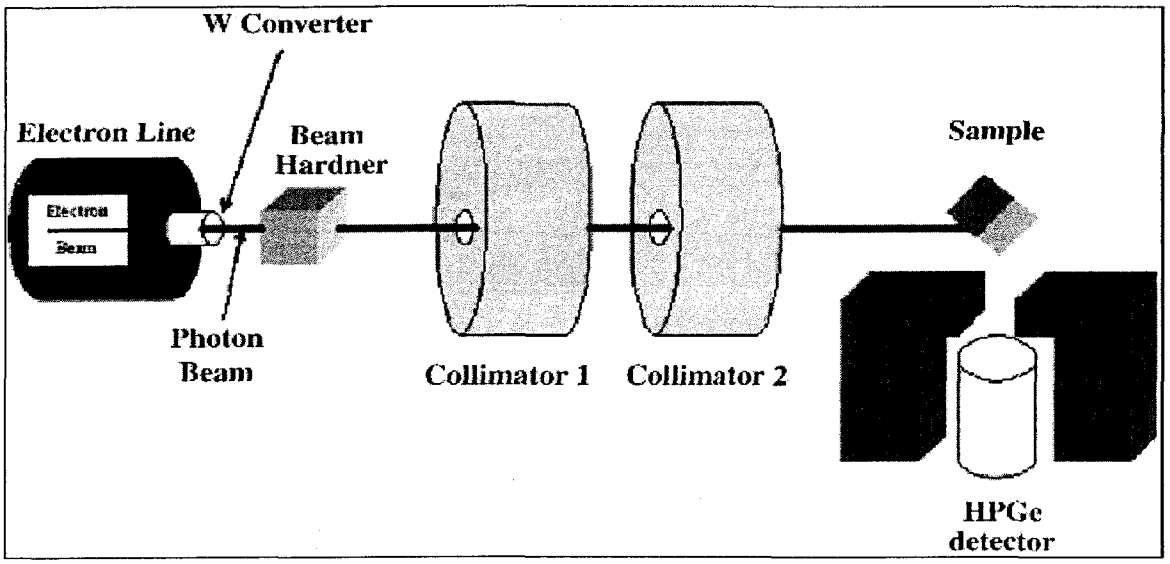

Figure 3.3 PAS Test Setup

3.2.2 Activation

The activation technique was based on the utilization of a photo-nuclear (υ, n) reaction involving a 20 MeV bremsstrahlung beam. Some of the resulting neutron-poor (proton-rich) nuclei, in turn, emitted positrons through a beta decay process. [23] The martensitic stainless steels studied in this investigation contained a substantial amount of iron, which generated positrons according to the photo-nuclear reactions given below. The positron generated by the activation technique was also thermalized and annihilated with the sample electrons emitting 2 photons in opposite direction having a 511 KeV energy spectrum. υ and n_o represent the gamma ray and neutron, and e^+ signifies positron.

$$^{54}Fe_{26} + \upsilon \longrightarrow {}^{1}n_0 + {}^{53}Fe_{26}$$

$$^{53}Fe_{26} \longrightarrow e^+ + {}^{53}Mn_{25}$$

The emitted photons were recorded in both the pair-production and activation techniques by a high purity Germanium (HPGe) detector, and the resultant data were analyzed in terms of three line- shape parameters such as S, W and T of the 511 KeV annihilation peaks, as shown in Figure 3.4. [24] The S and W parameters have often been used to characterize the annihilation peak in Doppler broadening spectroscopy. The S-parameter is sensitive to the annihilation with valence electrons and is defined as the ratio of counts in the central region of the peak to the total counts in the peak. The W-parameter is more sensitive to the annihilation with high momentum core electrons and is defined as the ratio of counts in the wing regions of the peak to the total counts in the peak. The T-parameter is simply the ratio of W to S. While the S-parameter is directly proportional to

the residual stress, the T-parameter is inversely proportional to the internal stress developed inside the test specimens. [25-27]

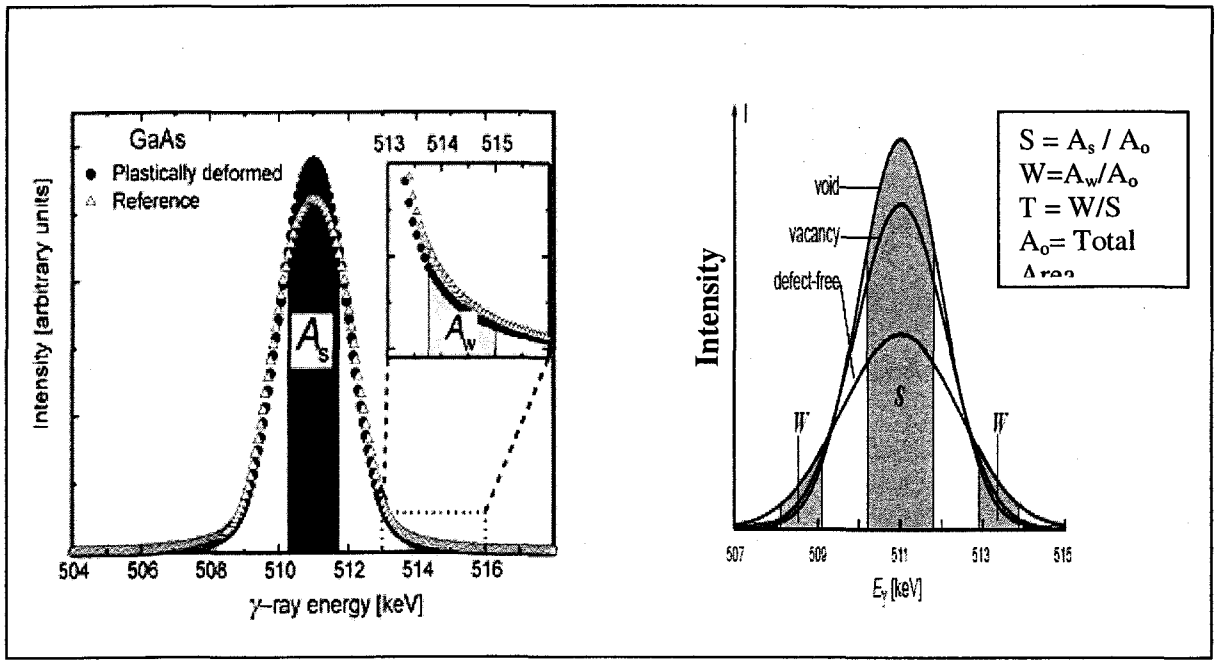

Figure 3.4 PAS spectrum showing S, W and T Parameters

3.3 Neutron- Diffraction

3.3.1 Operating Principles

The characterization of internal stresses by neutron diffraction (ND) is relatively a newer approach, which became available in the early 1980's in the United States, Germany, and Great Britain. A fair number of neutron-producing reactors exist now, that are well equipped for the determination of stresses by the ND technique. Some of the principal laboratories are RISO (Denmark), LANSCE (USA), ARGONNE (USA),

CHALK RIVER (Canada), HCR-ECN Petten (Holland), LLB Saclay (France), ISIS Rutherford (U.K).[28] However, the residual stress characterization of martensitic alloys used in this investigation was performed using the experimental facility located at the AECL, Chalk River Laboratory.

The ND technique is a well-established non-destructive method for the measurement of residual stress deep inside materials. Among the different existing techniques, only ND allows the 3D measurement of residual stresses inside a material achieved through translational and rotational movement of the component. The thermal neutrons are able to probe the atomic arrangement of the systems. A neutron scattering spectrometer allows measurement of the intensity of neutrons scattered from the sample as a function of the change in the energy and momentum of the neutrons. [15]

The principal advantage of using neutrons rather than the more conventional x-rays lies in the fact that the neutrons can penetrate deeper (3-4cm) into the metals to determine the internal stress.[29] The ND technique in general, is capable of penetrating approximately 1000 times deeper into the metal lattice compared to the x-ray diffraction method. The ND method relies on elastic deformations within a polycrystalline material that can cause changes in spacing of the lattice planes from their stress free value. The principle of strain measurement by ND is shown in the Figure 3.5

In the ND experiment, the neutron beam from the reactor was first monochromated to a chosen wavelength λ by Bragg reflection from a large single crystal monochrometer. This monochrometer beam was transmitted through a slit on the collimator, or by apertures, to pass over the 'sample axis' about which the detector was rotated.[30] The detector was used to count neutrons scattered through an angle of 2θ. The scattered beam

was then transmitted through the other collimator to the detector. The volume of the beam incident on the sample and the beam entering the detector was controlled by the height limiters made of cadmium

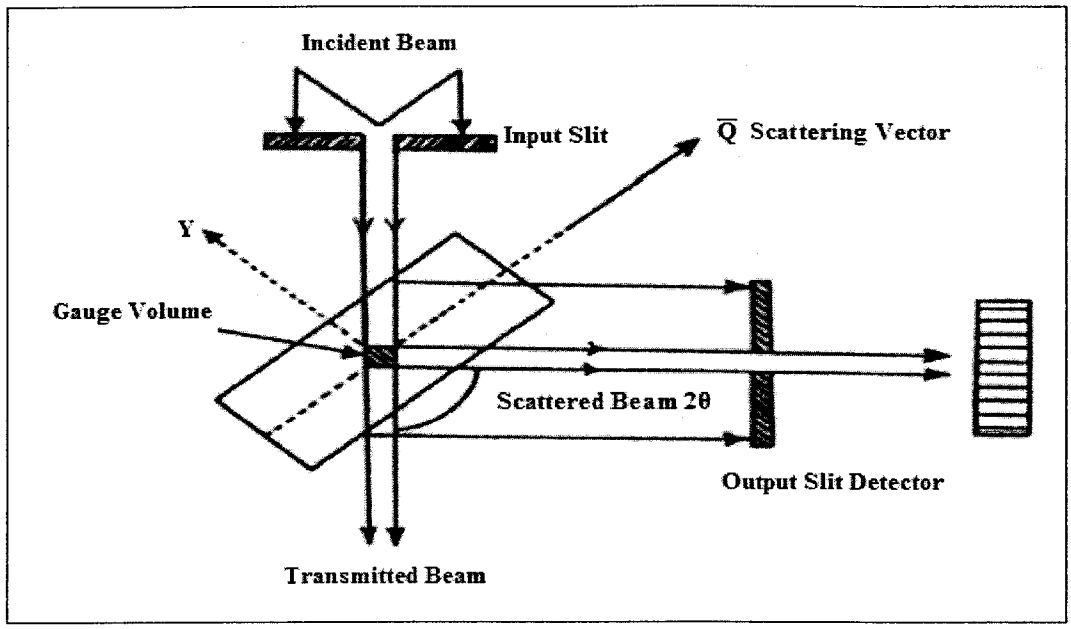

Figure 3.5 ND test set up

The 'gauge volume' or 'volume sampled' can be defined as the region developed due to the intersection of the incident and scattered beam as shown in Figure3.5. A sample, totally placed within this gauge volume, should enable the measurements of properties such as internal strain. The interplanar distance d_{hkl} where hkl are the Miller indices of the investigated lattice plane can be evaluated by using Bragg's law, given in equation 3.1.

$$\lambda = 2d_{hkl}\sin\theta \qquad \text{(Equation 3.1)}$$

where, λ = Neutron wavelength

2θ = Angle between the incident and the diffracted beam

d_{hkl} = Interplanar distance in a stressed material

The strain component lies along the bisector of the incident and diffracted beams. The sample can be oriented in different orientations, however the strain component lie along the bisector. The small lattice strain (ε_{hkl}) is given by the equation 3.2. [31]

$$\varepsilon_{hkl} = \frac{d_{hkl} - d_0}{d_0} \qquad \text{(Equation 3.2)}$$

Where d_o = hkl- interplanar distance in a stress-free material.

A small sample with measurements made in several orientations and averaged, or an extreme part of a component, may be taken to be in zero strain and taken as a reference sample. The variation of d_o due to compositional changes in material can also affect the results. [32]

Having measured the strain in a given direction, the stress is usually determined by first making the assumption that the material is isotropic, and then using the Young's modulus, E, and Poisson's ratio, ν, of the bulk material. These quantities must be accurately known for the material examined if the absolute stress has to be accurately determined. The values of E and ν are dependent on the lattice planes (hkl).The strain component which is constant over many grains are called macrostrains and are related to the macro-stresses by the equation of isotropic elasticity. In an elastic isotropic model the principal stresses are related to the strains by the following equations. [33]

$$\sigma_{xx} = \frac{E}{(1+\upsilon)(1-2\upsilon)}\left[(1-\upsilon)\varepsilon_{xx} + \upsilon\left(\varepsilon_{yy} + \varepsilon_{zz}\right)\right] \quad \text{(Equation 3.3)}$$

$$\sigma_{yy} = \frac{E}{(1+\upsilon)(1-2\upsilon)}\left[(1-\upsilon)\varepsilon_{yy} + \upsilon(\varepsilon_{xx} + \varepsilon_{zz})\right] \quad \text{(Equation 3.4)}$$

$$\sigma_{zz} = \frac{E}{(1+\upsilon)(1-2\upsilon)}\left[(1-\upsilon)\varepsilon_{zz} + \upsilon(\varepsilon_{xx} + \varepsilon_{yy})\right] \quad \text{(Equation 3.5)}$$

Where, E = Young's modulus

ν = Poisson's ratio

ε_{XX} = Strain in X-direction

ε_{YY} = Strain in Y-direction

ε_{ZZ} = Strain in Z-direction

Also, the uncertainity value in strain is related to the corresponding uncertainity in stress by using the following equation.

$$\Delta\sigma = \frac{E}{(1+\nu)} * \sqrt{\left(\frac{1}{1-2\nu}\right)\Delta\varepsilon_x^2 + \left(\frac{\nu}{1-2\nu}\right)^2\left(\Delta\varepsilon_{RD}^2 + \Delta\varepsilon_{ND}^2 + \Delta\varepsilon_{TD}^2\right)} \quad \text{(Equation 3.6)}$$

Where,

$\Delta\sigma$ = Uncertainty in Stress Value

ν = Poisson's Ratio

E = Young's Modulus

$\Delta\varepsilon_{RD}$ = Uncertainity in strain measured in the Rolling Direction

$\Delta\varepsilon_{ND}$ = Uncertainity in strain measured in the Normal Direction

$\Delta\varepsilon_{TD}$ = Uncertainity in strain measured in the Transverse Direction

$\Delta\varepsilon_{\chi}$ = Uncertainity in the Principal Direction, where X= RD, ND or TD

3.3.2 Experimental Facility

A neutron scattering spectrometer allows measurement of the intensity of neutrons scattered from the sample as a function of the change in the energy and momentum of the neutrons. In general, instruments used for elastic scattering measurements, to investigate the time-averaged atomic structure within a sample, are called diffractometers and those used for inelastic scattering measurements, to investigate the excitation spectrum of the atomic structure, are called spectrometers. The measurement devices included a spectrometer, detector and two collimators. The spectrometer was provided with neutrons from the reactor core. The test specimens were mounted on to the measuring device by means of special fixtures. The testing facility used consisted of a large-capacity X-Y table that could handle loads upto 450 kg (1,000lbs) and provided a large 60 cm × 60 cm (2" × 2") platform for easy mounting of multiple samples as shown in Figure 3.6. The test sample was aligned properly with a computer-controlled X, Y and Z translators to a very accurate sampling volume at the required location within the specimen. The collimated neutron beam which impinges on the sample gets diffracted and this diffracted beam was recorded by a detector. The detector moves around the sample and in this case it is a 32-wire position sensitive detector. [34] This detector can also be used as a variable single-channel detector. A stress rig for examining the specimens under uniaxial load (tension

and compression) can be used to determine the diffraction elastic constants for which the rig can be placed on the spectrometer on both the Young's and Poisson orientations. The maximum applied load was 45 kN (5 tons). The sampling volume of the neutron beam that impinged on the test sample was defined by various height limiters made of cadmium.

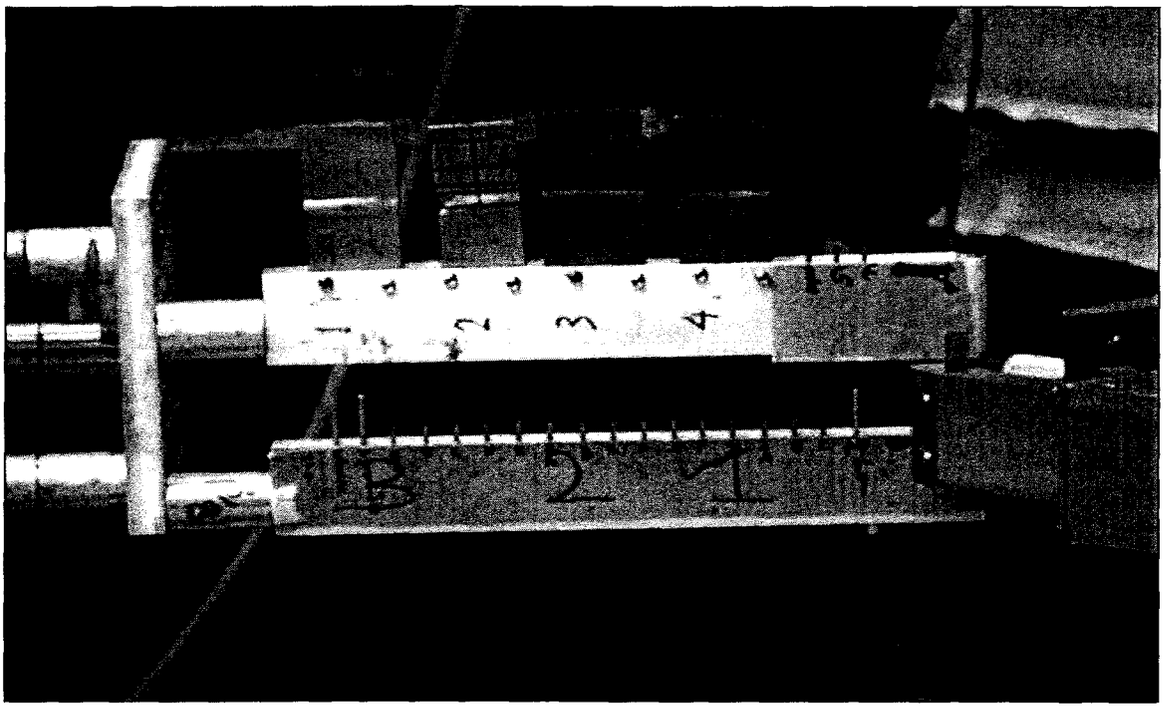

Figure 3.6 Mounting of Multiple Samples

3.4 Scanning Electron Microscopy

In a scanning electron microscope (SEM), electrons from a metal filament are collected and focused, just like light waves, into a narrow beam. The beam scans across the subject, synchronized with a spot on a computer screen. Electrons scattered from the

subject are detected and create a current, the strength of which makes the spot on the 25 computer brighter or darker. This creates a photograph-like image with an exceptional depth of field. Magnifications of several thousand times are possible in SEM. Normally, SEM provides black and white micrographs. Analysis of failure in metals and alloys involves identification of the type of failure. The test specimens were sectioned into ½ to 3/4 of an inch in length to accommodate them in the vacuum chamber of the SEM.

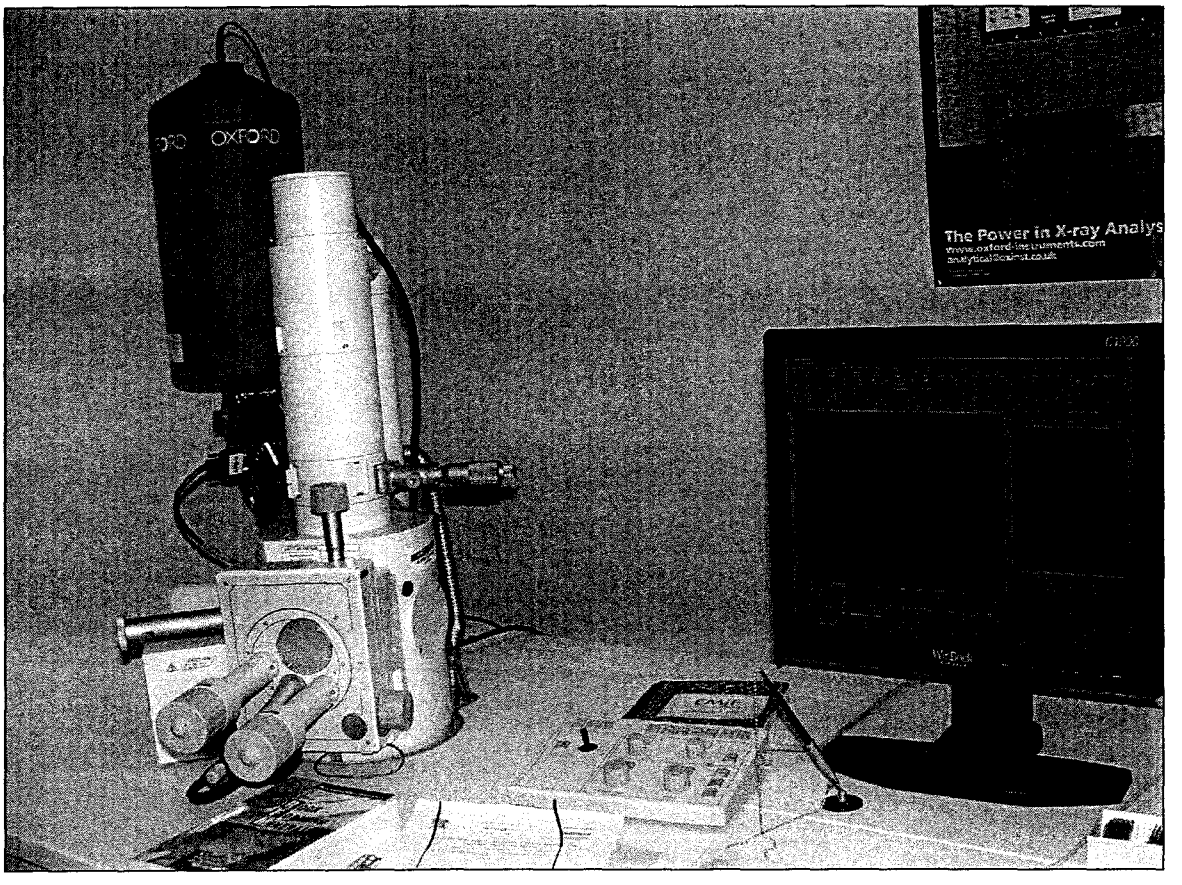

Figure 3.7 Scanning Electron Microscope

Usually, failure can occur by one or more of the several mechanisms, including surface damage, such as corrosion or wear, elastic or plastic deformation and fracture. Failures can be classified as ductile or brittle. Dimpled microstructure is a characteristic of ductile failure. Brittle failure can be of two types, intergranular and transgranular. An intergranular brittle failure is characterized by crack propagation along the grain boundaries while a transgranular failure is characterized by crack propagation across the grains. A JEOL-5600 SEM was used in this investigation to analyze the morphology of failure of the tested specimens. [35] The scanning electron microscope used for this investigation is shown in the Figure 3.7.

3.5 Optical Microscopy

The characterization of metallurgical microstructures of the test specimens before and after testing by optical microscopy is of primary importance. The principle of an optical microscope is based on the impingement of a light source perpendicular to the test specimen. The light rays pass through the system of condensing lenses and the shutters, up to the half-penetrating mirror. This brings the light rays through the objective to the surface of the specimen. Light rays reflected off the surface of the sample then return to the objective, where they are gathered and focused to form the primary image. This image is then projected to the magnifying system of the eyepiece. The optical microscope used in this investigation is shown in the Figure 3.8. The micrograph results from either an inherent difference in intensity or wavelength of the light absorption characteristics of the phases present. It may also be induced by preferential staining or attack of the surface by etching with a chemical reagent. The test specimens were sectioned and mounted

using the standard metallographic technique, followed by polishing and etching to reveal the microstructures including the grain boundaries. The polished and etched specimens were rinsed in deionized water, and dried with acetone and alcohol prior to their

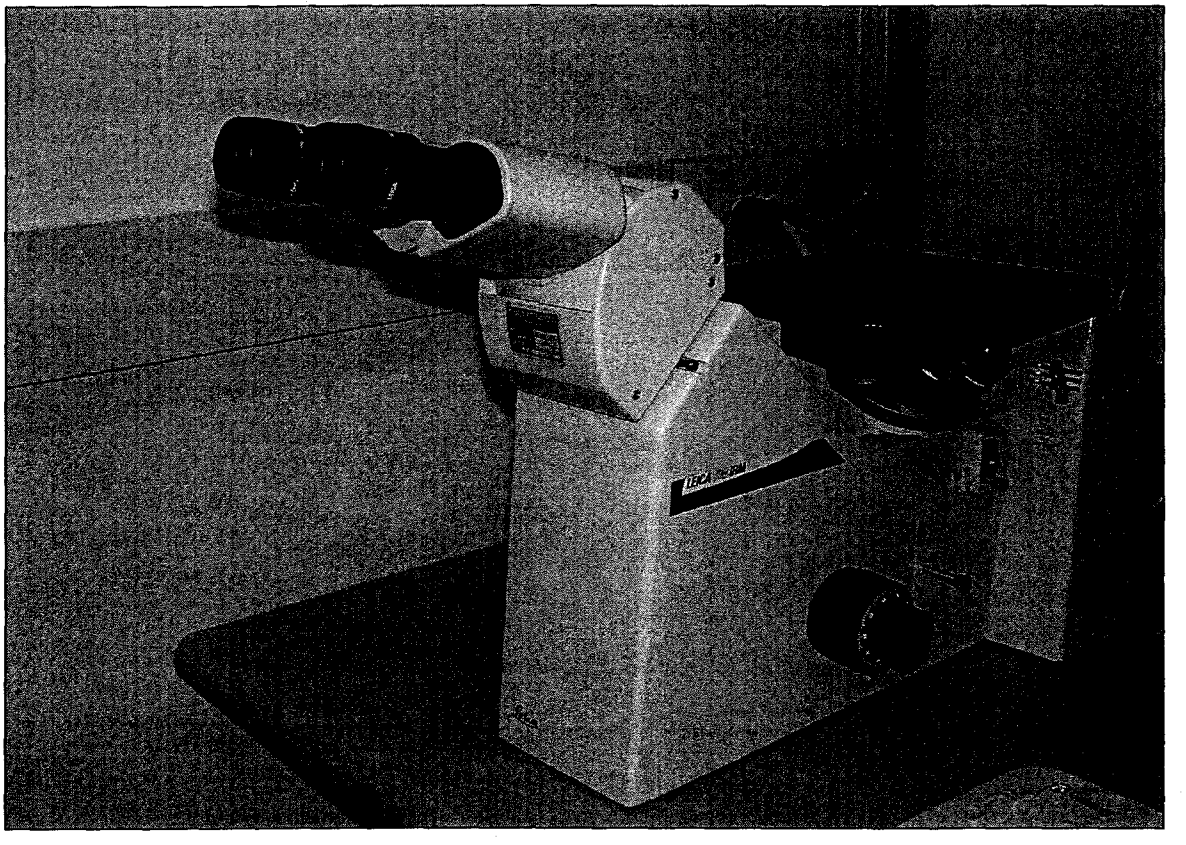

Figure 3.8 Optical Microscope

evaluation by a Leica optical microscope, having a resolution of up to 1000X.[36]

3.6 Transmission Electron Microscopy

In a TEM, a thin specimen was irradiated with an electron beam of uniform current density. The electron energy is in the range of 300 keV. Electrons are emitted in the electron gun by thermionic emission from tungsten cathodes. A condenser-lens system permits the area of the specimen to be illuminated and the specimen is imaged

onto a fluorescent screen. The dislocation density corresponding to the different levels of CR was calculated by using the line intersection method, [37,38,39] which was based on the superimposition of a grid consisting of horizontal and vertical lines on the TEM micrograph containing dislocations, as illustrated in Figure 3.10. The magnitudes of the total length of the horizontal (ΣL_h) and vertical (ΣL_v) test lines were determined from the test grid, while the thickness (t) of the TEM specimen was determined by electron energy loss spectroscopy [40] using Equation 4.1. Finally, the dislocation density (ρ) was calculated using Equation 4.2. The typical TEM used in this investigation is shown in the Figure 3.10

$$t = \lambda \ln (I_t/I_o) \qquad \text{(Equation 3.7)}$$

$$\rho = \frac{1}{t}\left(\frac{\sum n_v}{\sum L_v} + \frac{\sum n_h}{\sum L_h}\right) \qquad \text{(Equation 3.8)}$$

Where,

I_t = total intensity reaching the spectrometer

I_o = zero-loss intensity reaching the spectrometer

λ = mean free path

Σn_v = No. of intersections of vertical test lines with dislocations

Σn_h = No. of intersections of horizontal test lines with dislocations

ΣL_h = Total length of horizontal test lines (meter)

ΣL_v = Total length of vertical test lines (meter)

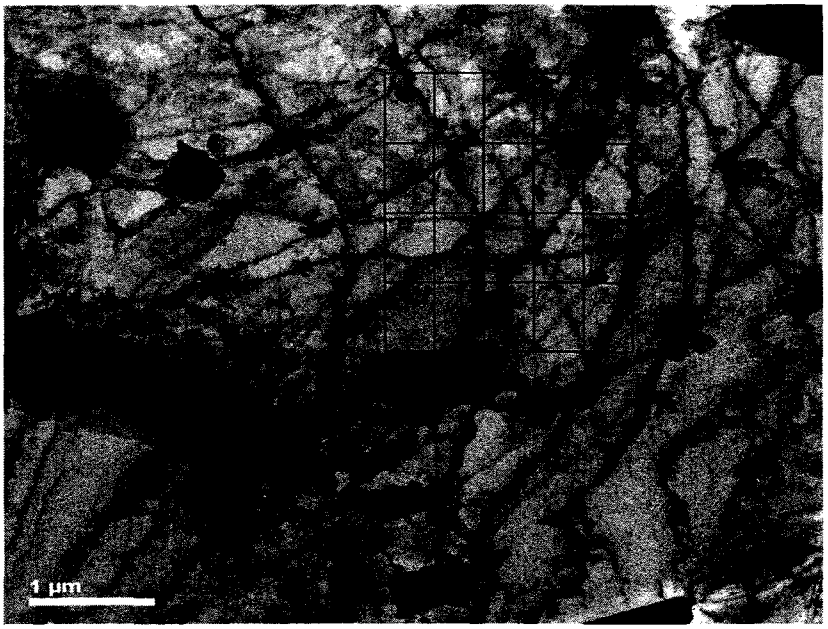

Figure 3.9 TEM Micrograph of Alloy EP-823 used to Determine ρ by Line Intersection Method

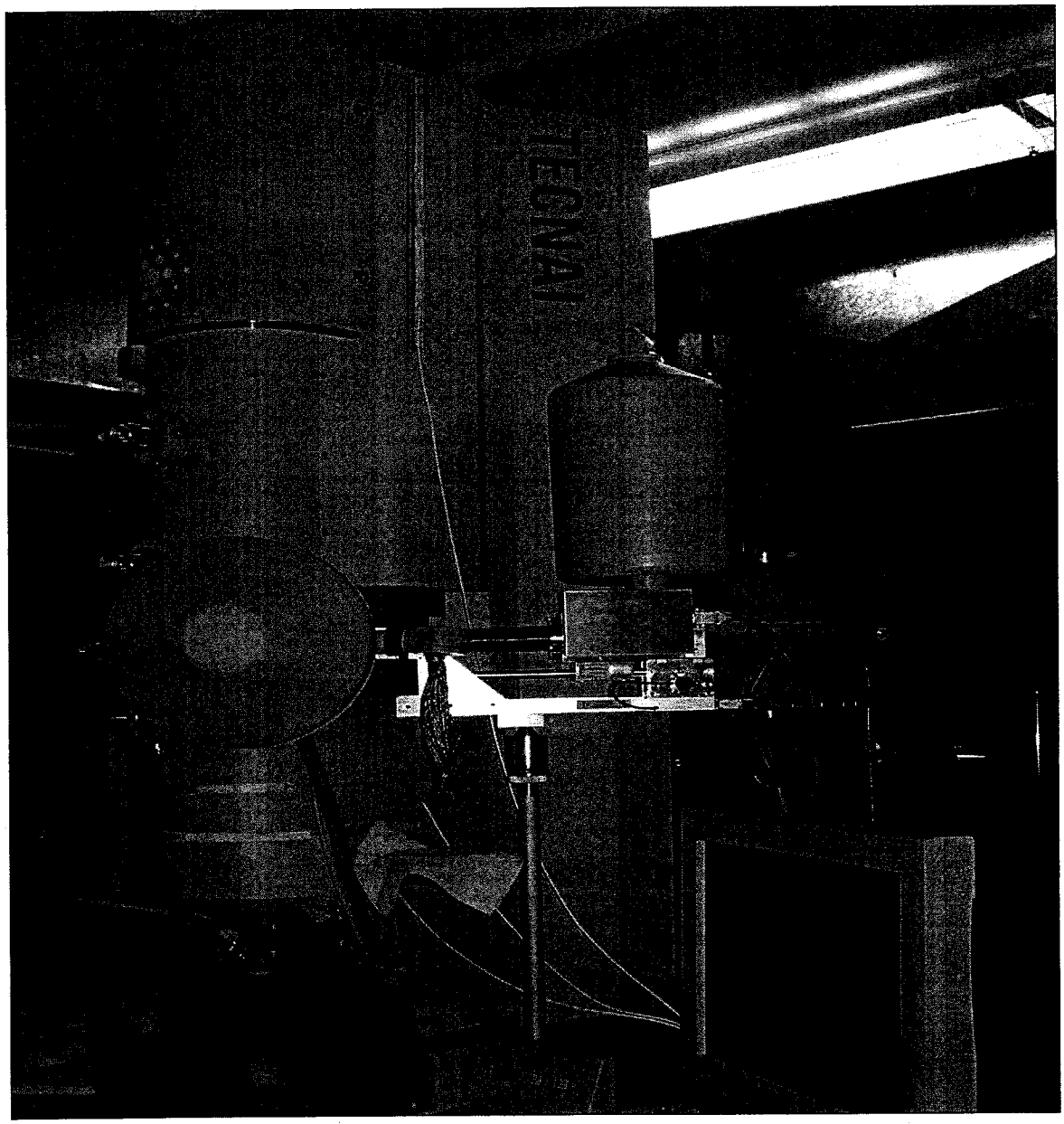

Figure 3.10 Transmission Electron Microscope

CHAPTER 4

RESULTS

As indicated earlier in this thesis, this investigation is focused on the characterization of residual stress in different types of specimens by neutron diffraction (ND), and two techniques such as activation and pair production based on the classical positron-annihilation-spectroscopy (PAS). Martensitic Alloys EP-823 and HT-9 were subjected to cold deformation by rolling, plastically deformed by tensile loading and welded using similar and disimilar materials on either side of the weld. The effect of post-weld-thermal-treatment (PWTT) on the resultant residual stress in the welded specimens was also investigated. The metallographic and fractographic evaluations of the tested specimens were performed by optical microscopy and scanning electron microscopy (SEM). Since the plastic deformation of structural materials can lead to the generation of defects such as dislocations, transmission electron microscopy (TEM) was also used to characterize dislocations and their densities. The resultant data based on the overall testing activities are presented in the following subsections.

4.1 Metallurgical Characterization and Tensile Properties evaluation.

The metallurgical microstructures of both tested materials, evaluated by conventional metallographic techniques, are shown in Figures 4.1 and 4.2. They were

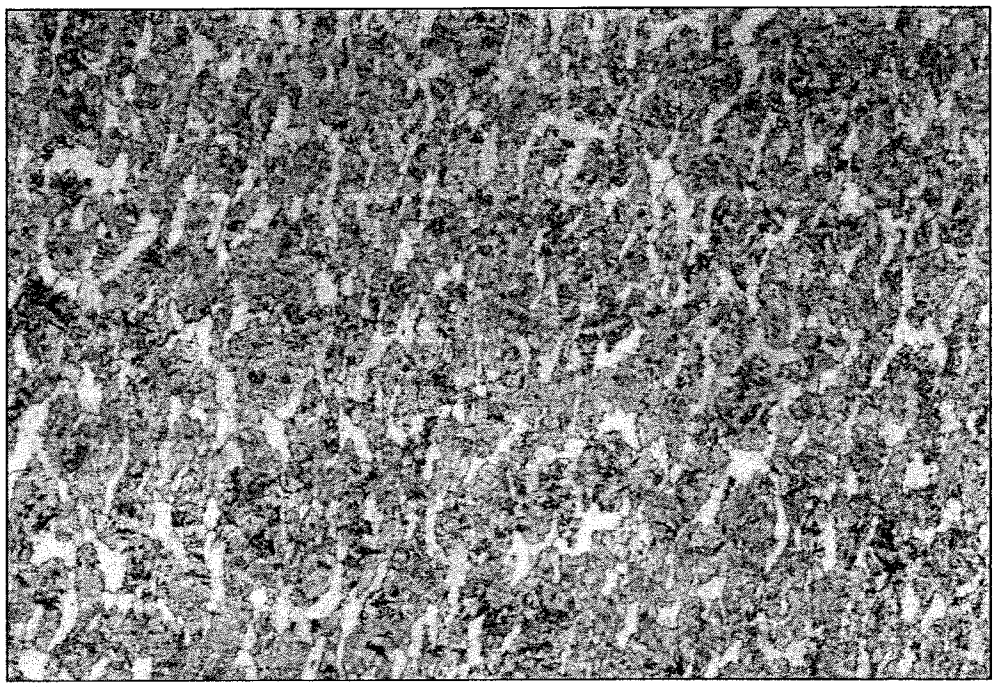

Figure 4.1 – Optical Micrograph of Q&T Alloy HT-9, Fry's Reagent, 100X

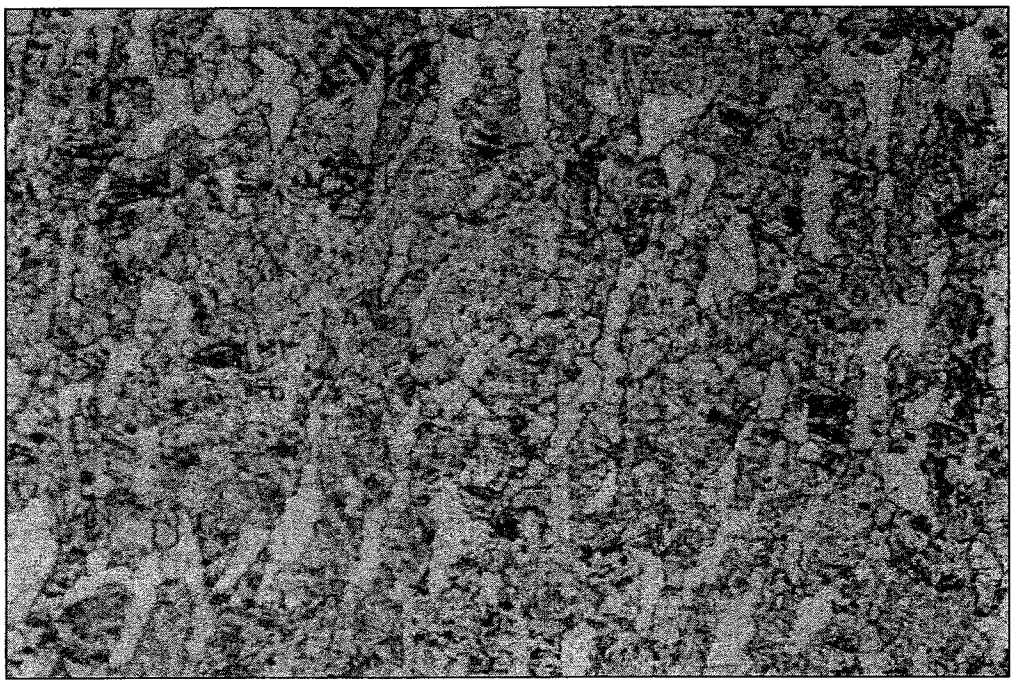

Figure 4.2 – Optical Micrograph of Q&T Alloy EP-823, Fry's Reagent, 100X

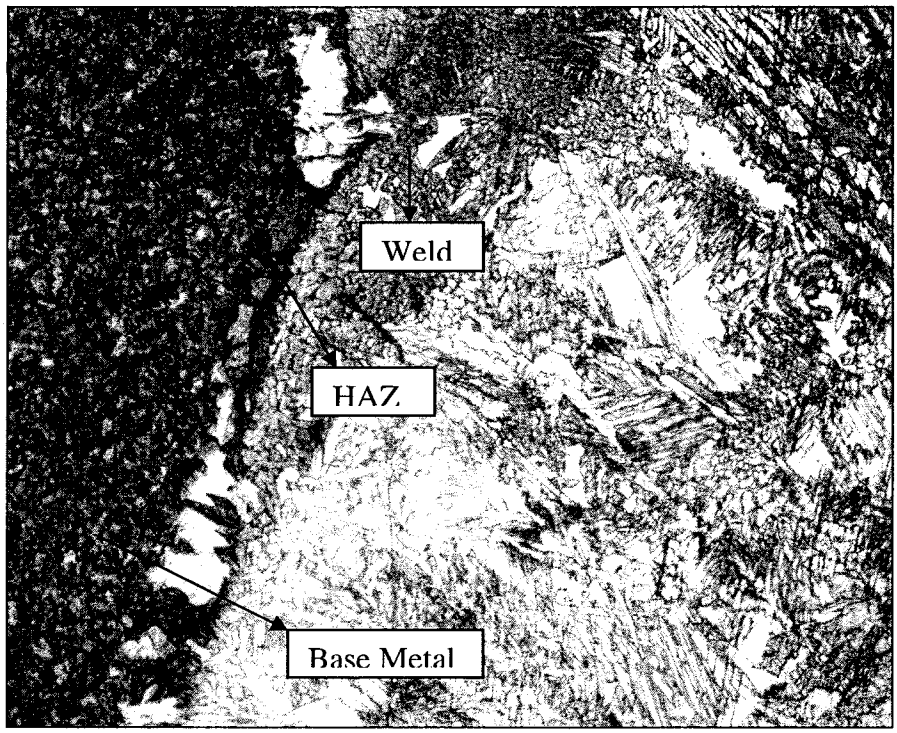

Figure 4.3 Optical Micrograph of HT-9/HT-9 Welded Specimen
Fry's Reagent, 100 X

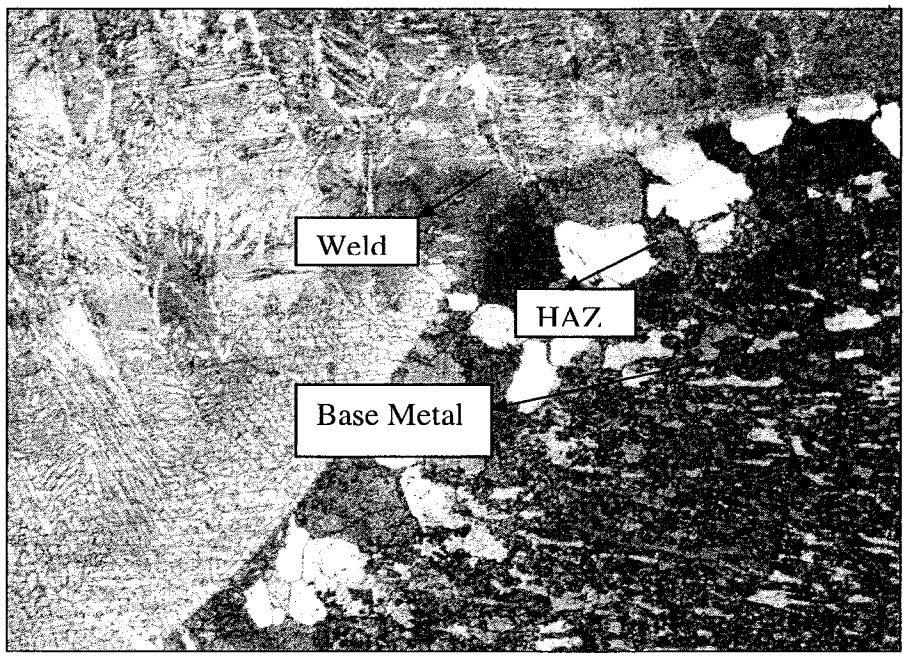

Figure 4.4 Optical Micrograph of HT-9/HT-9 Welded Specimen
Fry's Reagent, 100 X

etched by using Fry's reagent which contained 5 gm of cupric chloride ($CuCl_2$), 40 ml of HCl, 25 ml of ethanol (C_2H_5OH), and 30 ml of water (H_2O). An examination of these optical micrographs revealed fine grained tempered martensitic microstructures having some delta ferrites. The metallurgical microstructures of the welded specimens, showing the different regions including the weld, heat- affected- zone (HAZ) and base metal are illustrated in Figures 4.3 and 4.4, respectively for HT-9/HT-9 and HT-9/EP-823 welded specimen.

The results of tensile testing at room temperature are given in Table 4.1, showing the magnitude of the yield strength (YS), the ultimate tensile strength (UTS), the percent elongation (%El) and the percent reduction in area (%RA). It is interesting to note that while the ductility in terms of %El and %RA was identical for both alloys, comparatively lower strength was observed with Alloy EP-823, possibly due to the reduced carbon (C) content in this Alloy. However, the silicon (Si) content in this Alloy was substantially higher, as given in table 2.2 [41] the different regions including the weld, heat-affected zone (HAZ) and base metal are illustrated in Figures 4.3 and 4.4, respectively for HT-9/HT-9 and HT-9/EP-823 welded specimen.

Table 4.1 – Room-temperature Tensile Properties of Test Materials

Material / Heat No.	Thermal Treatments	YS Ksi (MPa)	UTS ksi (MPa)	% El	% RA
Alloy EP-823/2360	Quenched and Tempered (Q & T)	97 (669)	121 (835)	25	61
Alloy HT-9/2361		105 (724)	138 (952)	25	61

4.2 Residual Stress Measurements by ND

4.2.1 Cold-Worked Specimens

Alloy HT-9 and Alloy EP-823 were subjected to reduction in thickness by desired amount applying the cold-rolling operation. Even though, it was desired to give similar levels of cold-deformation to the plate materials of both alloys, the magnitudes of the resultant reductions were somewhat different. Alloy HT-9 resulted in reduction in thickness by 5.7 and 14.8 % respectively. On the other hand, Alloy EP-823 exhibited cold-reduction levels of 6.3 and 12.7 %, respectively. These cold-reduced specimens were then tested by ND for evaluation of the magnitude of the resultant residual stresses corresponding to different levels of deformation as a function of the depth of the specimen. ND measurements were also performed on materials without any cold-reduction.

The distributions of residual stresses in Alloy HT-9, with and without cold reduction, as measured by the ND technique are illustrated in Figure 4.5(a, b and c). An examination of Figure 4.5(a) indicates that the magnitude of residual stress in Alloy HT-9 without any cold-reduction was very negligible showing insignificant variation in tensile and compressive residual stresses through out the thickness of the plate material. It is interesting to note that the extent of residual stress at the top and bottom surface of Alloy HT-9, cold reduced by 5.7 and 14.8 %, respectively, were tensile in nature as shown in Figure 4.5(b and c). However, at some intermediate depth, within the specimen thickness the residual stress was compressive in nature indicating that the magnitude of residual stress was significantly higher at the top and bottom surfaces of the specimen compared to that of the inner regions. A similar observation was also made for Alloy EP-823 for

three levels (0, 6.3, 12.7%), of cold-reduction of respectively, as illustrated in Figure 4.6(a, b and c). It should be noted that the insignificant amount of residual stresses in both alloys, shown in Figures 4.5(a) & 4.6(a) without any cold-reduction may be the results of prior plastic deformation imparted to them before their thermal treatments. The experimental variables such as eccentricity of the beam, the angle of incidence and the unstressed interplanar distance may play significant roles in providing the width of error-bands in both the ND and PAS experimental techniques.

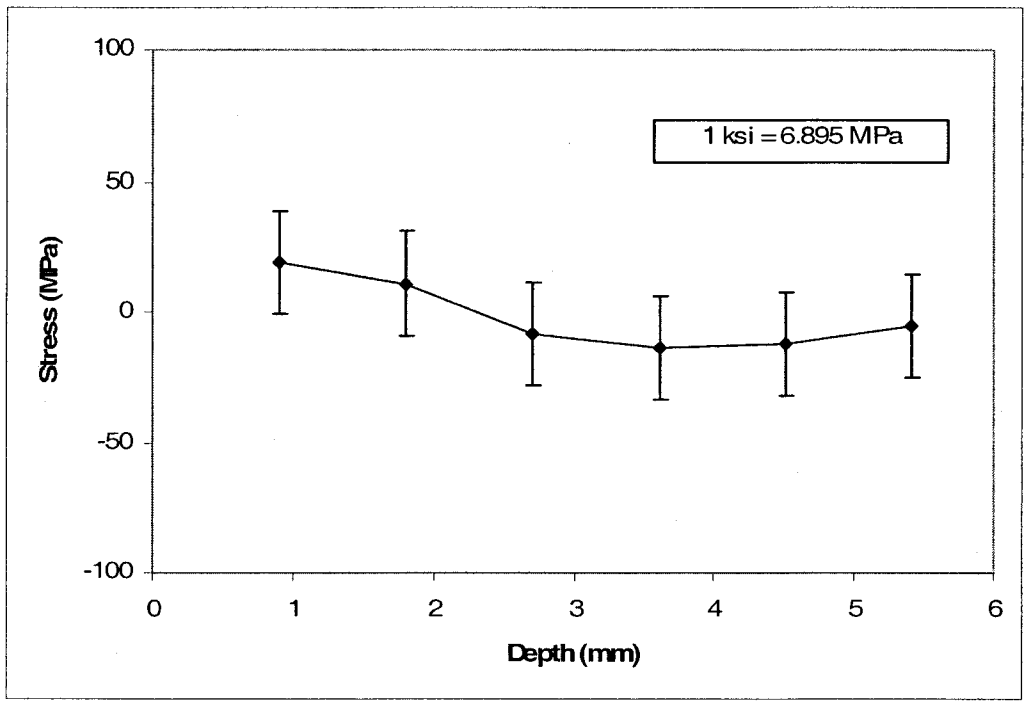

(a) With No Cold-Reduction

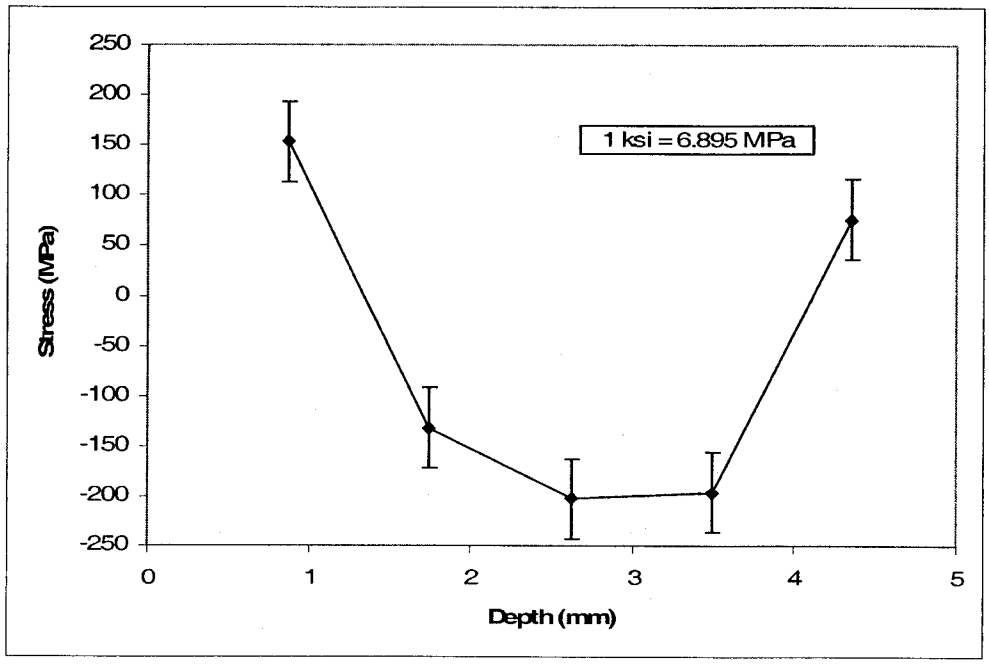

(b) 5.7% CR

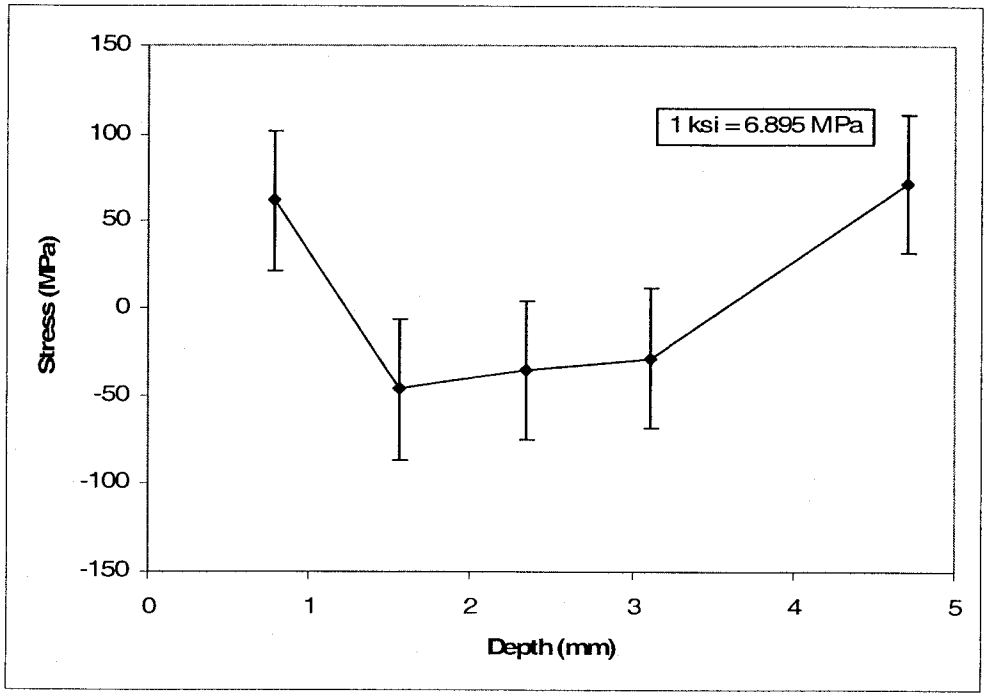

(c) 14.8% CR

Figure 4.5 Variation of Residual Stress vs. Depth in Alloy HT-9

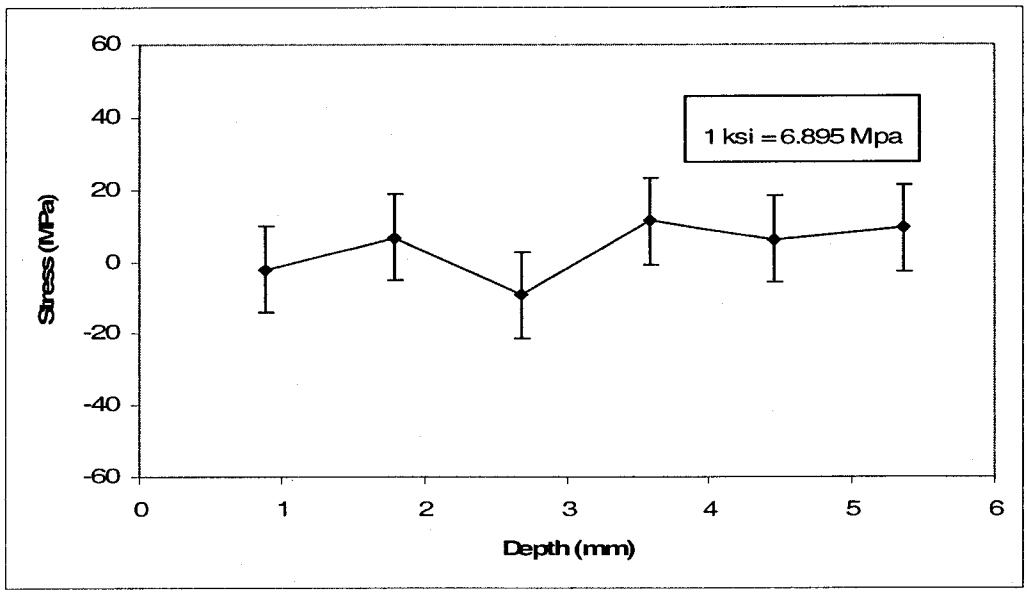

(a) with no cold-reduction

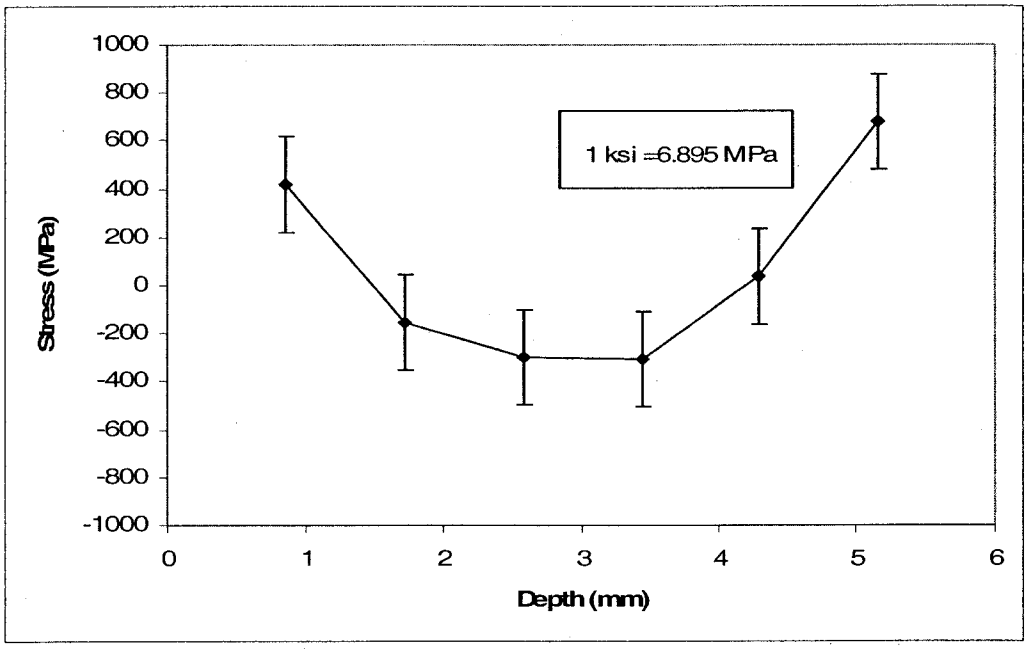

(b) 6.3% CR

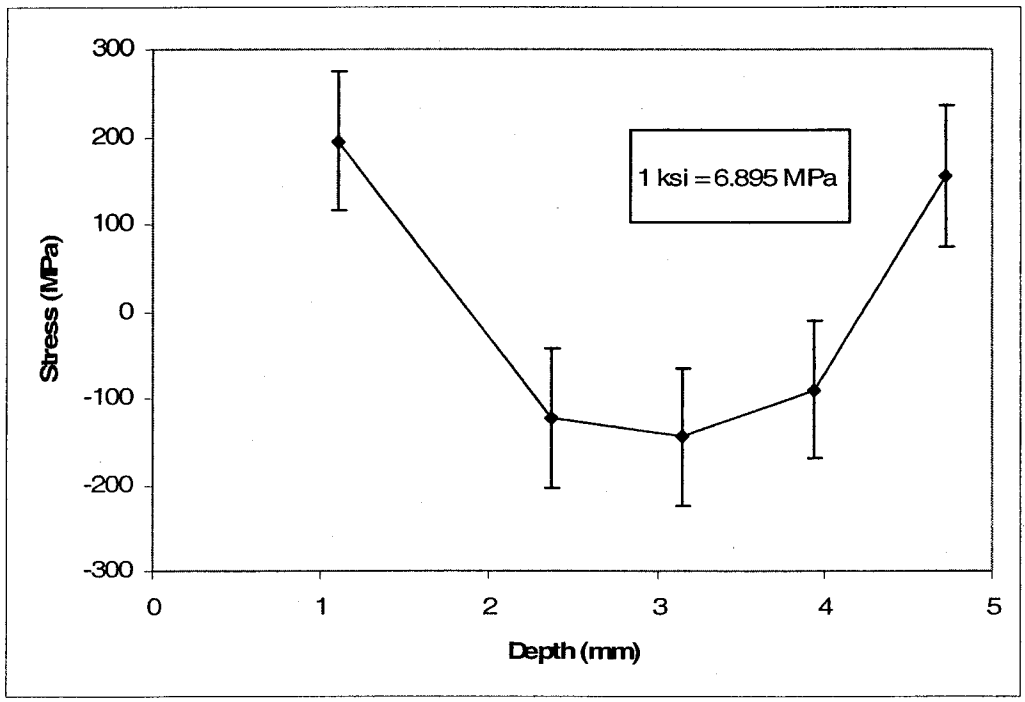

(C) 12.7 % CR

Figure 4.6 Variation of Residual Stress vs. Depth in Alloy EP-823

4.2.2 Plastically-deformed Cylindrical Specimens

Cylindrical specimens, of Alloy EP-823 plastically deformed at different tensile stress levels ranging between YS and UTS were evaluated by the ND technique for determination of residual stress corresponding to different applied tensile stresses. Measurements were made at one surface of the gage section of the cylindrical specimen and at a location 4mm inside the gage section of the specimen. The magnitudes of residual stresses determined at both locations by the ND technique are shown in Figure 4.7 as a function of the applied tensile stress varying from YS to UTS. An examination of this figure clearly demonstrates a gradual enhancement in residual stress as the applied stress was increased by some specified amount between YS and UTS.

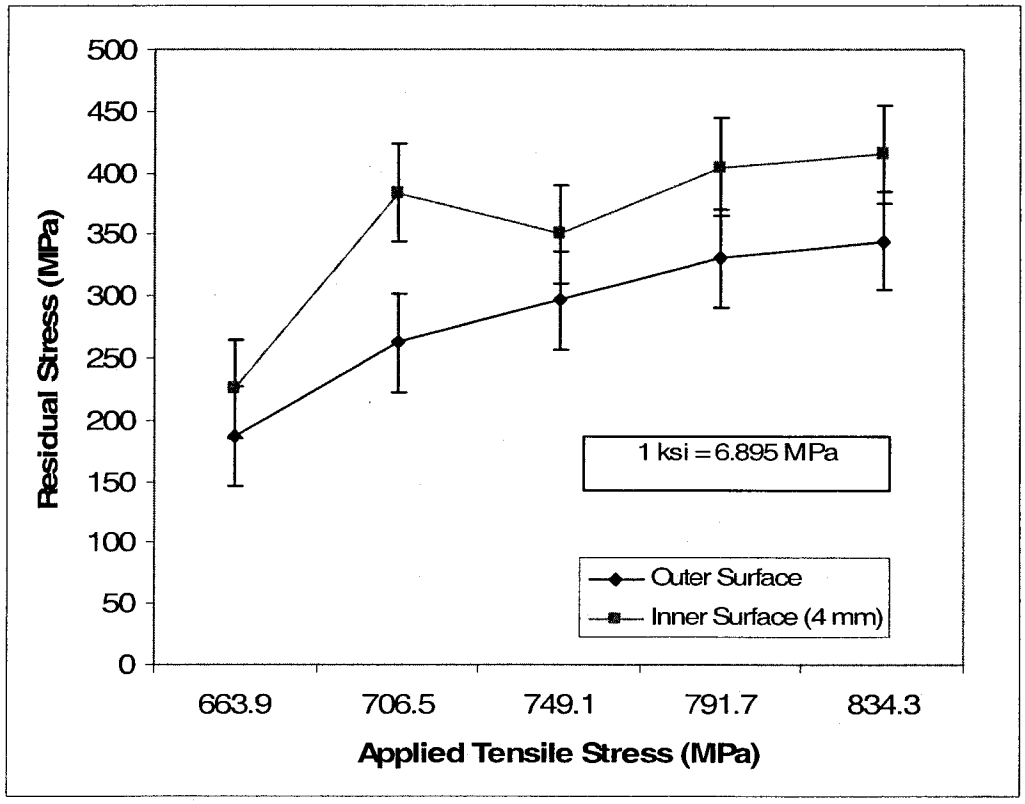

Figure 4.7 Applied Tensile Stress vs. Residual Stress

4.2.3 Welded Specimens

ND measurements were performed on welded specimens consisting of similar and disimilar martensitic alloys (HT-9/HT-9, HT-9/EP-823). These measurements were performed at a depth of 2mm from the surface but 7, 10 and 18mm away from the center of the welded region. The measured residual stresses in both alloys are shown in Figures 4.8 through 4.10 as a function of the distance (7, 10, 18 mm) from the center of the weld. It is obvious from these results that the magnitude of residual stress was reduced away from the welded region, as expected. It is well known that the maximum residual stress can be developed close to the fusion line due to rapid solidification rate in this region, which may gradually be reduced with distance away from it.

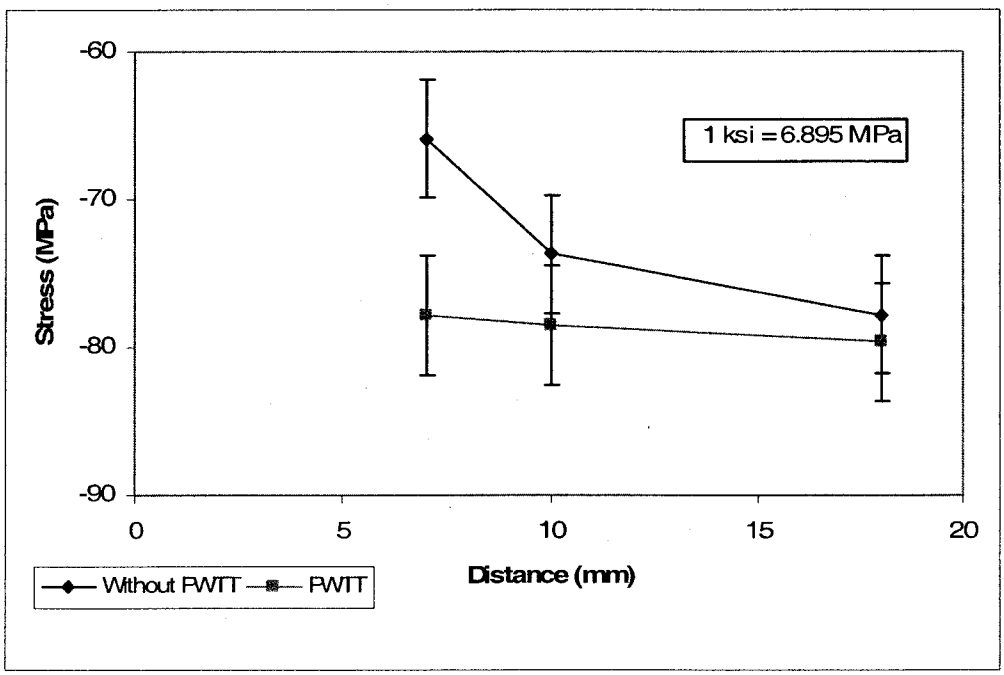

Figure 4.8 Residual Stress Profile in HT-9/ HT-9 Welded Specimen

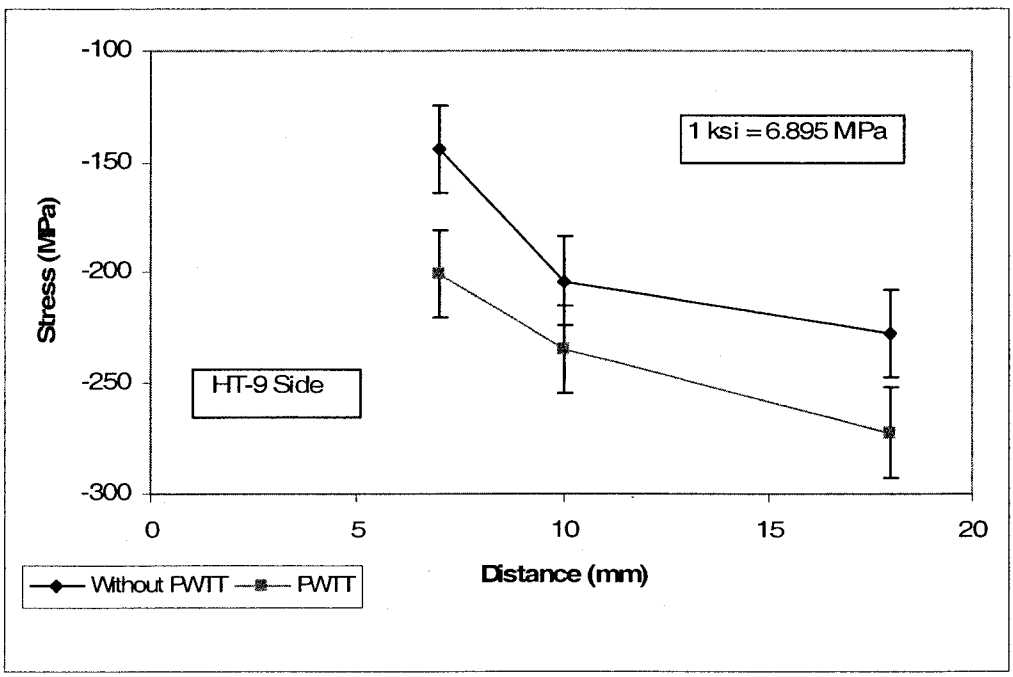

Figure 4.9 Residual Stress profile in HT-9/EP-823 Welded Specimen (HT-9 Side)

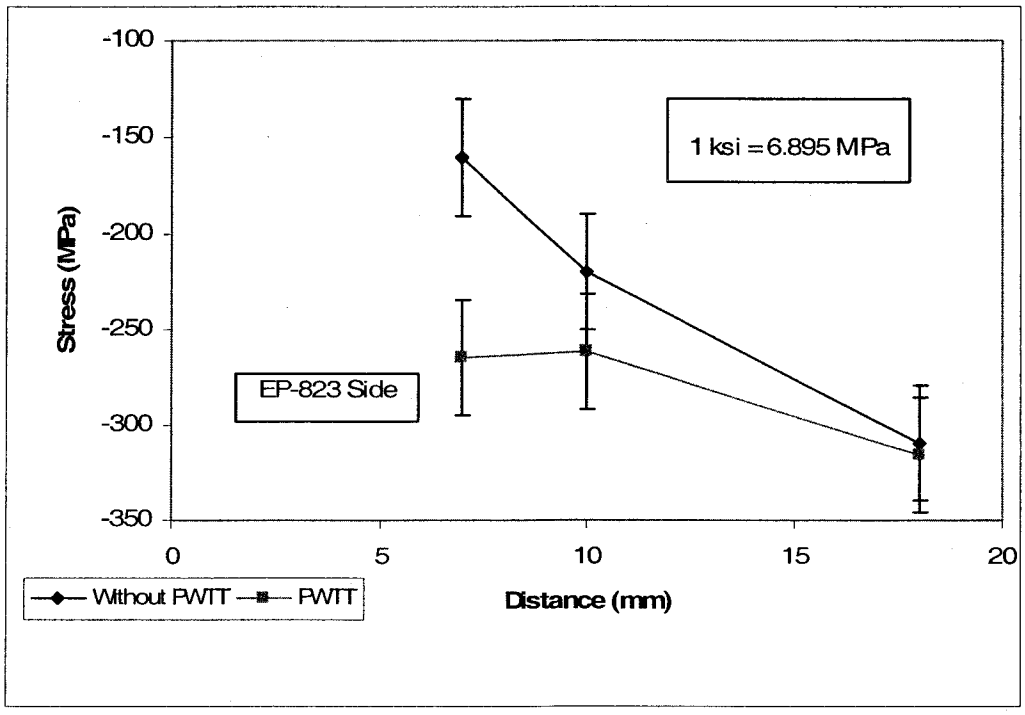

Figure 4.10 Residual Stress profile in HT-9/EP-823 Welded Specimen (EP-823 Side)

It is customary to relieve the resultant internal stresses by thermal treatment which is commonly known as post-weld-thermal-treatment (PWTT). In order to investigate the effect of PWTT, ND measurements were also performed on the same welded specimens subjected to PWTT. A comparison of the resultant residual stresses at an identical depth, and distances due to PWTT is illustrated in Figure 4.8 through 4.10. This comparison clearly demonstrate a benificial effect of PWTT, showing reduced internal stresses at comparable distances due to stress relief by specific thermal treatment described in a previous section.

4.3 Residual Stress Measurements by PAS

Efforts were made to compare the estimated residual stress in both martensitic alloys by activation and pair-production techniques in terms of the PAS line-shape-parameters S, W and T. The following sub-sections present the results obtained from activation and pair-production, respectively.

4.3.1 Evaluation of Cold-worked specimens by Activation

The results of residual stress characterization by activation on cold-worked HT-9 specimens subjected to different levels of cold-reduction by rolling are illustrated in Figure 4.11 (a, b and c). The extent of residual stress at different levels of cold-reduction is shown in this figure in terms of S, W and T-parameter based on the annihilation peak. An evaluation of these data reveals that the internal stresses developed due to cold-reduction was enhanced at higher cold-reduction level, characterized by increased S-Parameter value. On the contrary, the magnitude of W and T-parameter was gradually reduced at higher cold-reduction levels. However, at highest level of cold-reduction the trend was opposite. The data indicate that the extent of residual stress was maximum in specimens subjected to intermediate level of cold-reduction. The enhanced residual stress at this intermediate reduction level may be due to the larger driving force needed to promote the dislocation movement associated with plastic-deformation. Once these dislocations move past the grain boundary, reduced stresses might be needed that can account for further deformation. Thus, the resultant data are consistent in that, the magnitude of S-parameter was directly proportional to the internal stress, while the W

and T-parameters were inversely proportional to the residual stress. A similar observation was also made with Alloy EP-823, as illustrated in Figure 4.12 (a, b and c).

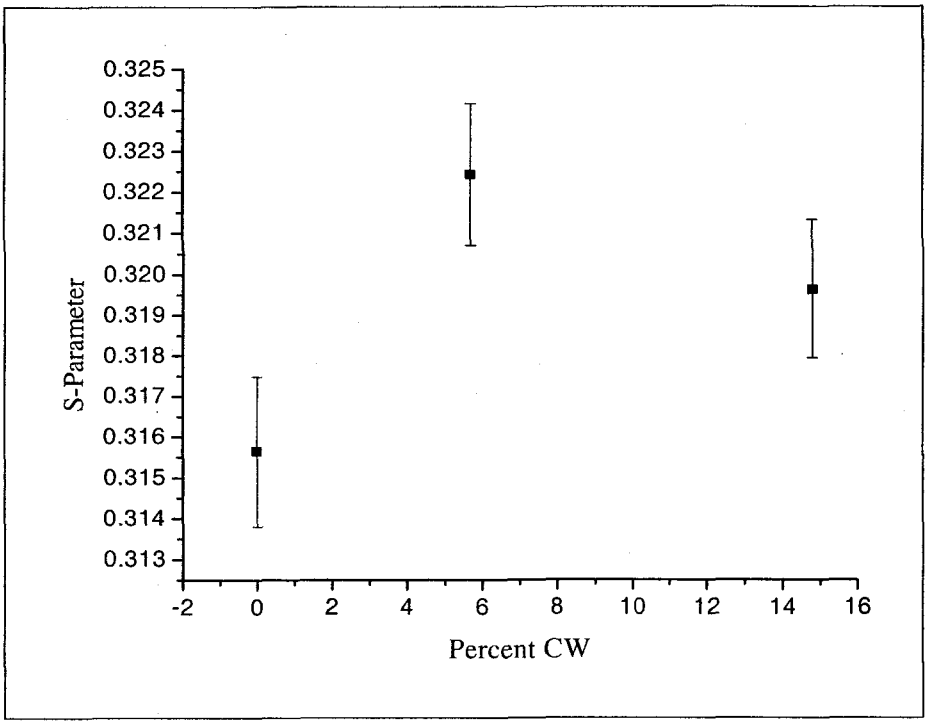

(a)

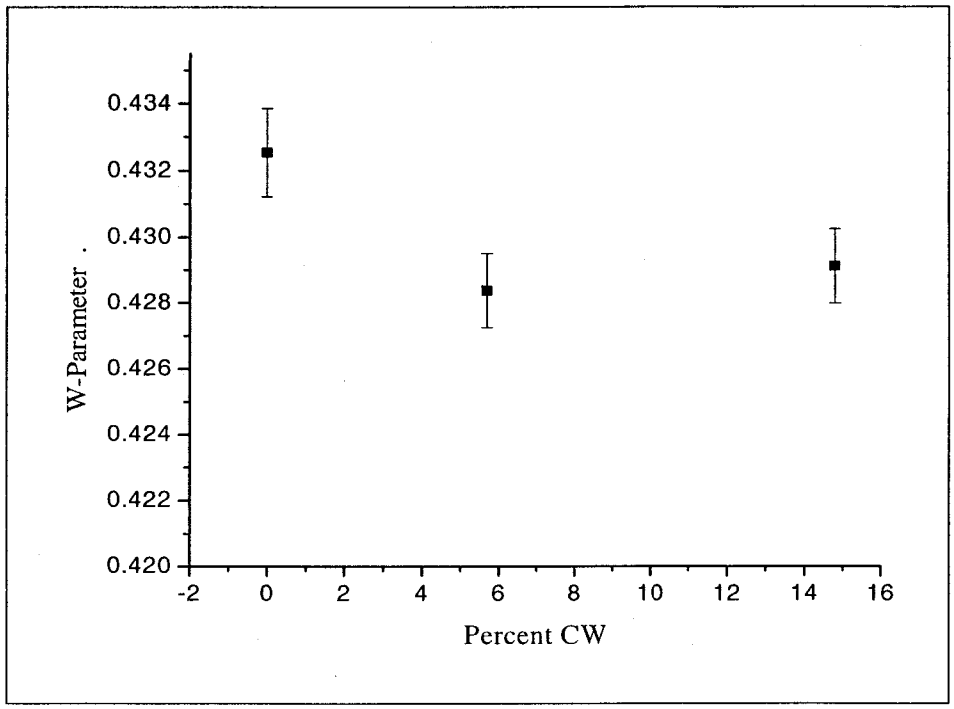

(b)

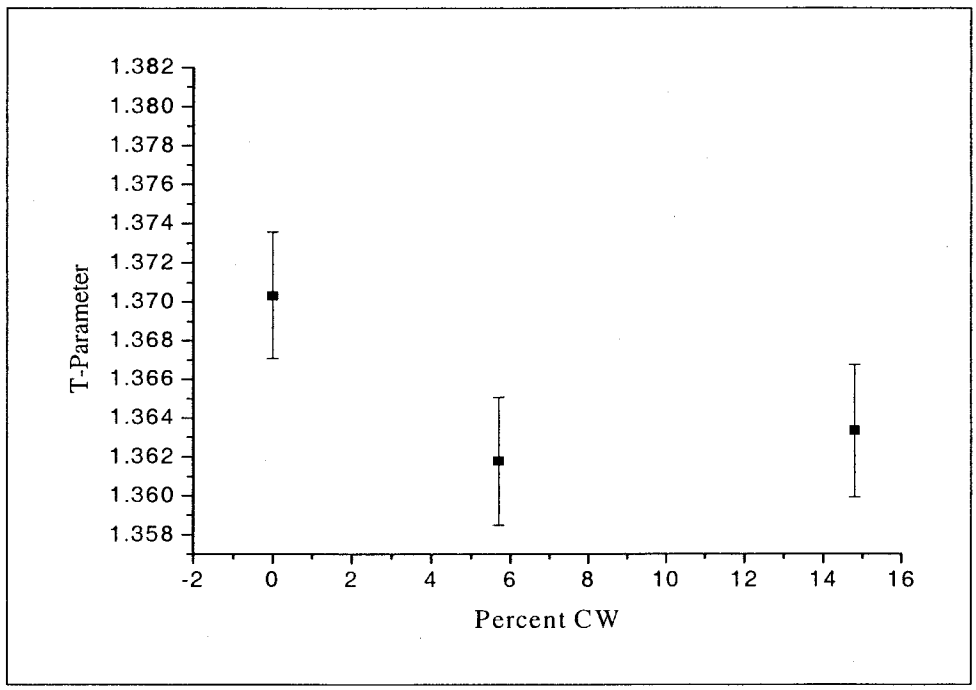

(c)

Figure 4.11 S, W and T-Parameter vs. Percent CW for Alloy HT-9 (Activation)

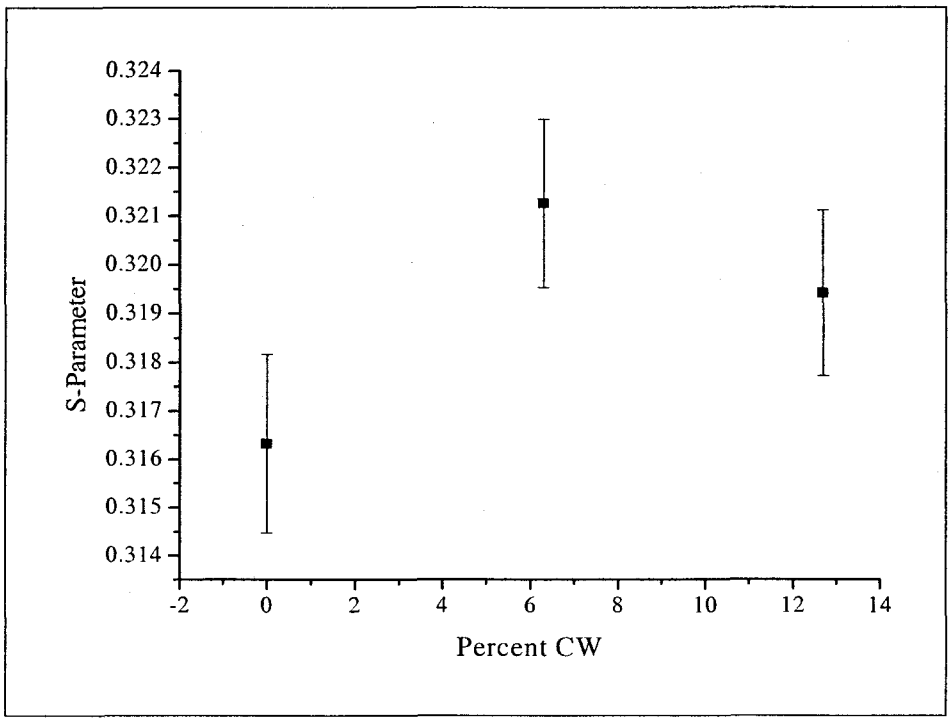

(a)

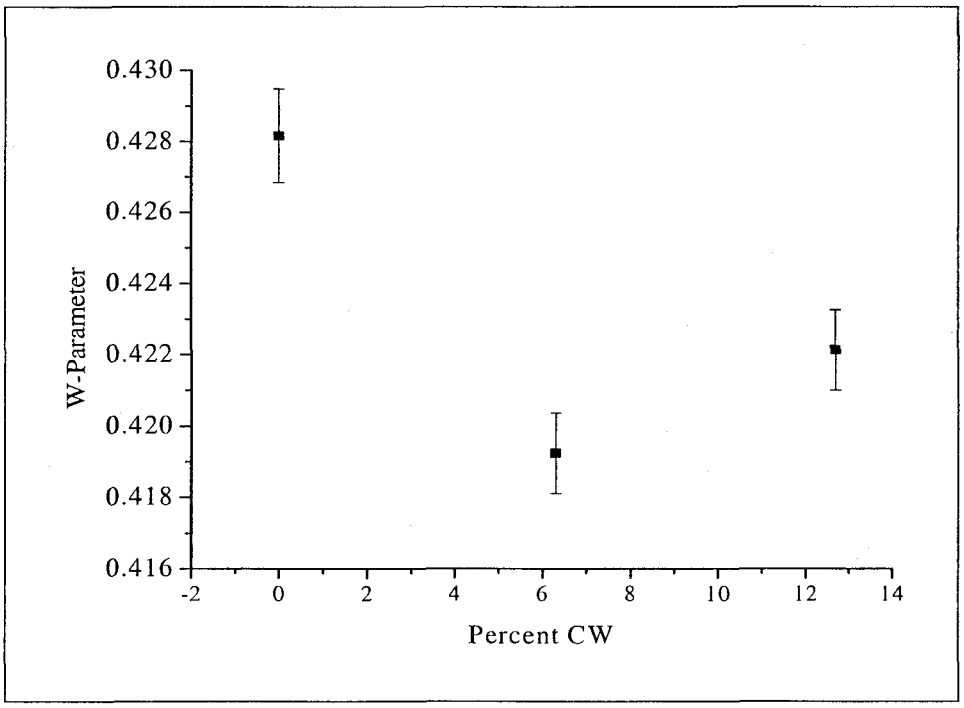

(b)

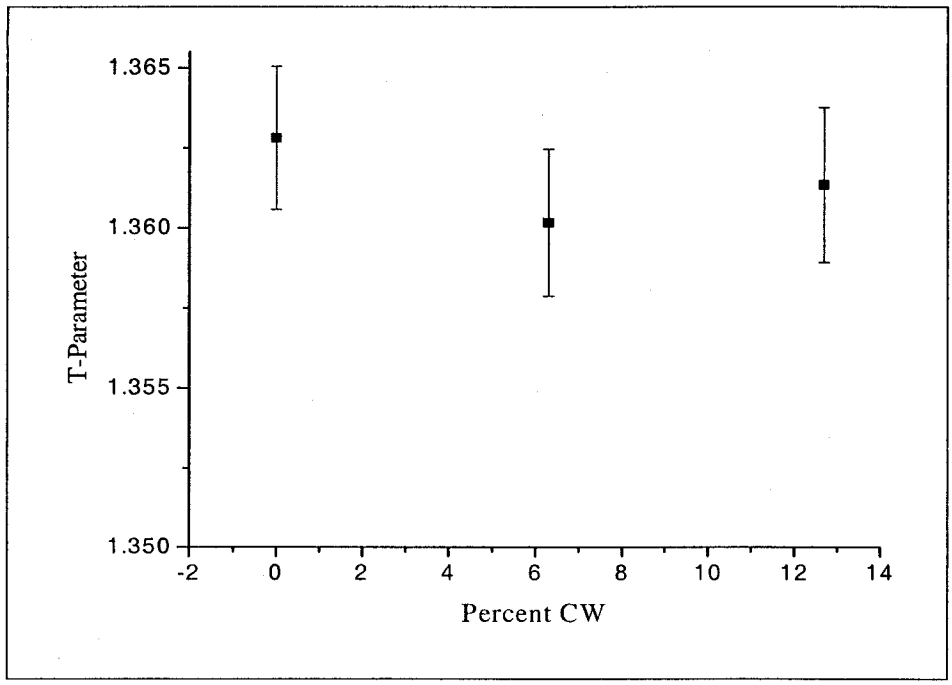

(c)

Figure 4.12 S, W and T-Parameter vs. Percent CW for Alloy EP-823 (Activation)

4.3.2 Evaluation of Cylindrical Specimens by Activation.

The results of residual stress characterization of Alloy HT-9 by Activation on cylindrical specimens subjected to plastic deformation by tensile loading at three different applied stress levels (104.55,121.25,137.95 ksi) are illustrated in Figure 4.13 (a, b and c). Once again, the S-Parameter was gradually increased with increasing applied stress level, indicating higher internal stresses. Simultaneously the W and T-Parameters were gradually reduced with increasing applied stress, suggesting higher residual stress. Similar trends on the effect of applied stress on these three parameters were also noted for Alloy EP-823, except for the fact that the magnitudes of applied stresses were

different (96.3, 102.475, 108.65, 121 ksi). The variation of S, W and T-Parameters with applied stress for Alloy EP-823 are shown in Figure 4.14 (a, b and c).

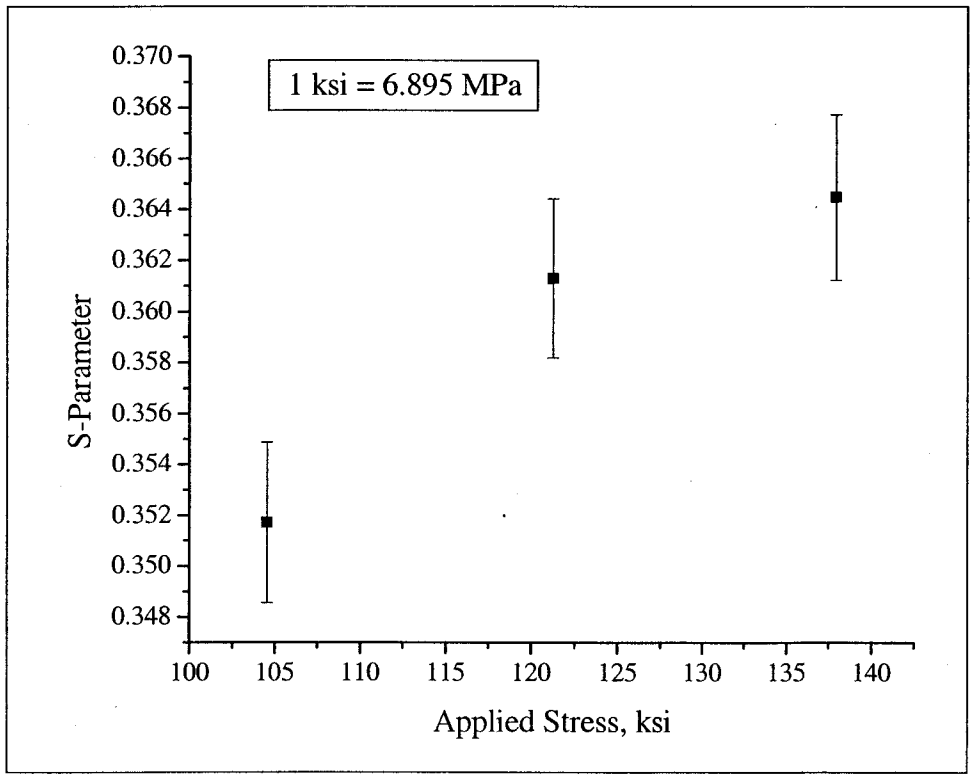

(a)

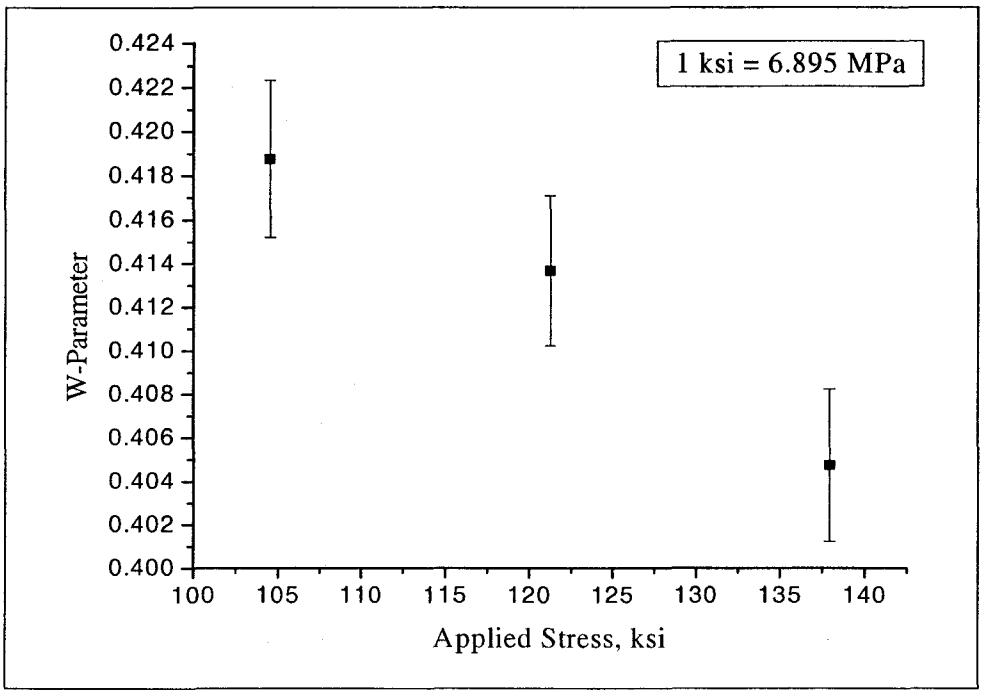

(b)

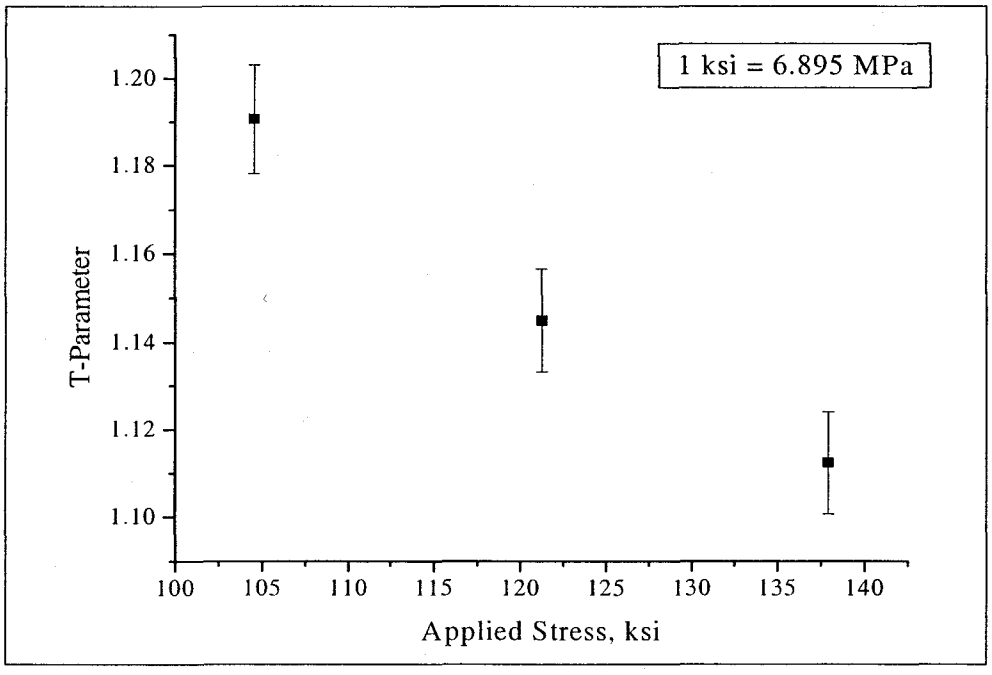

(c)

Figure 4.13 – S, W, and T-Parameter vs. Applied Stress for Alloy HT-9 (Activation)

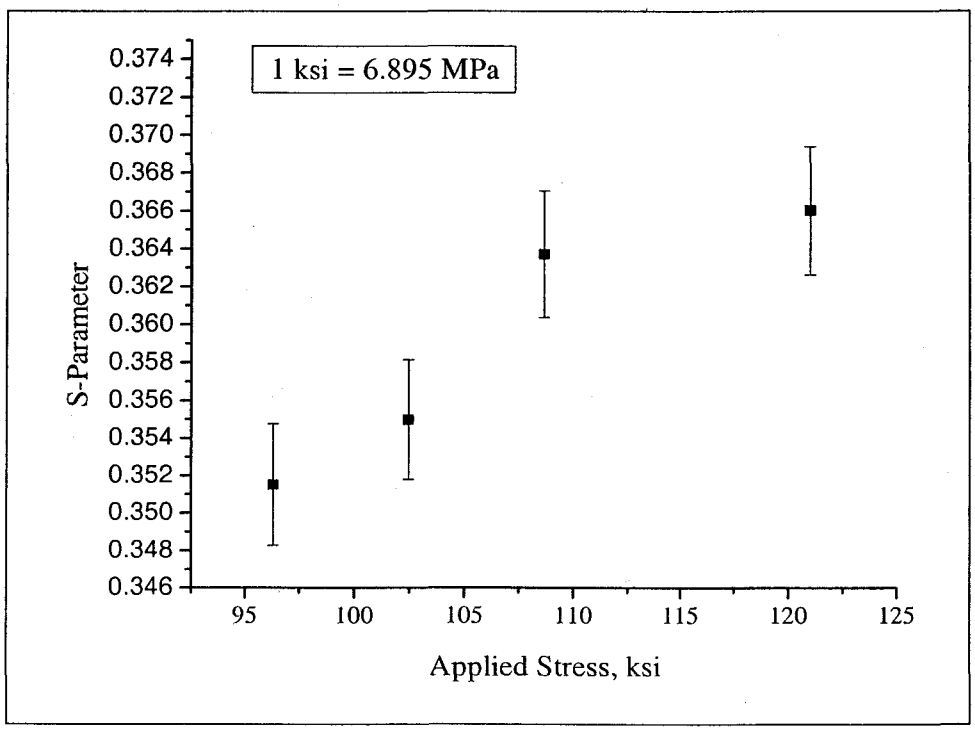

(a)

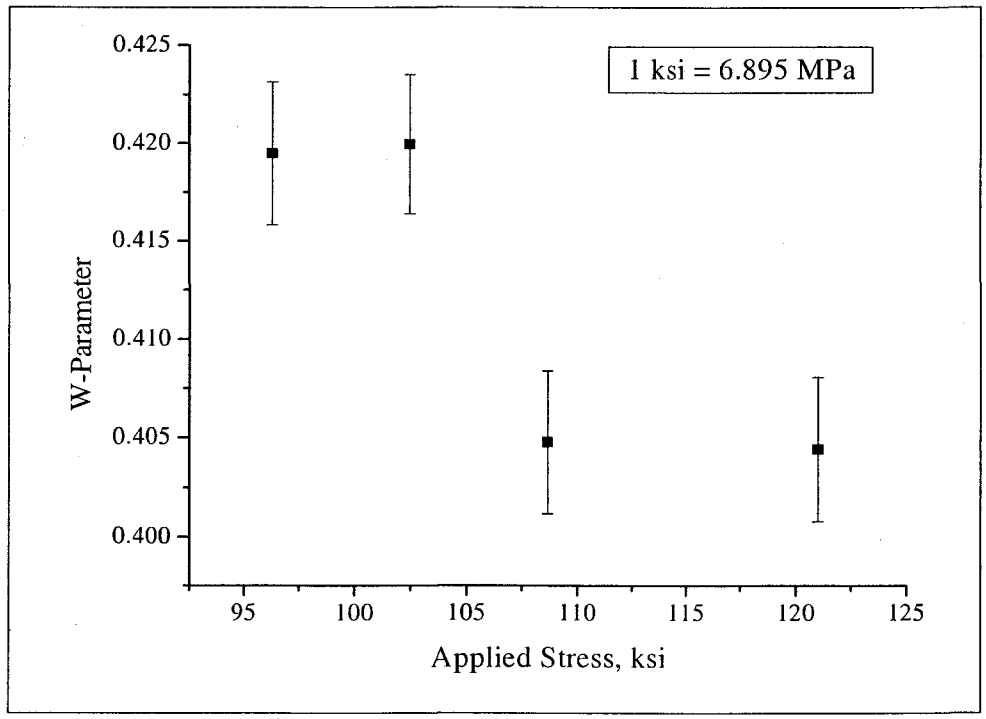

(b)

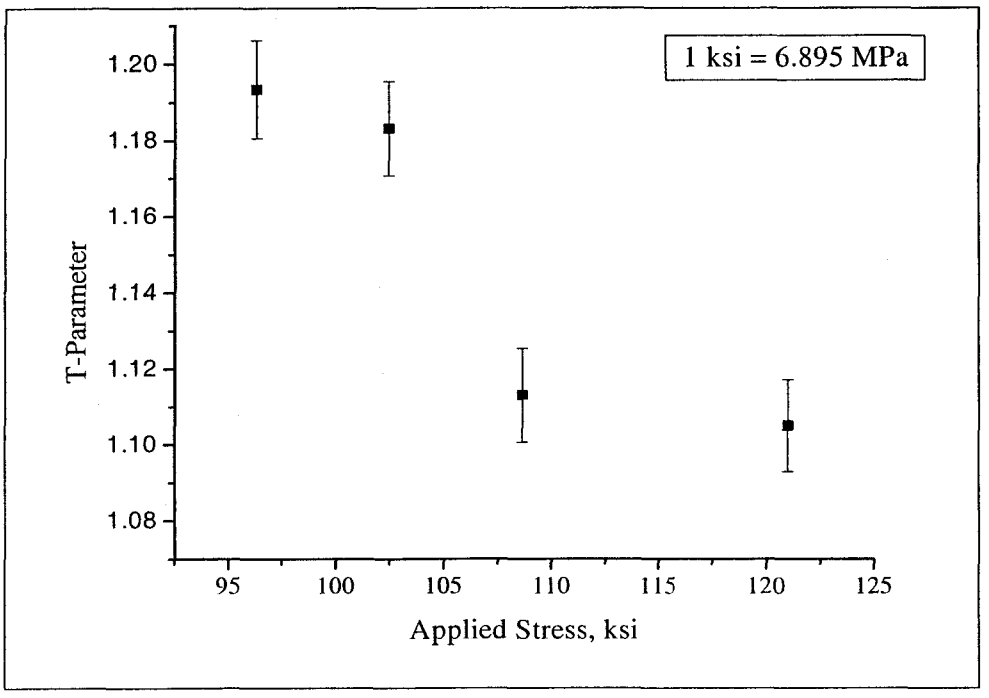

(c)

Figure 4.14 – S, W, and T -Parameter vs. Applied Stress for Alloy EP-823 (Activation)

4.3.3 Evaluation of Cold-worked Specimens by Pair-Production

The magnitudes of residual stresses generated in cold-worked specimens of Alloy HT-9 subjected to different levels of cold-reduction, determined by the pair-production method, are shown in Figure 4.15 (a, b and c) in terms of S, W and T- parameters. Consistent with prior observations, the S-Parameter was gradually enhanced with increasing cold-reduction levels. Simultaneously both W and T parameters were gradually reduced with increased levels of cold-reduction. The enhanced S-parameter indicated higher residual stresses. On the other hand, the reduced W and T-parameter signified enhanced internal stresses with increased cold-reduction as expected. However, at the highest cold-reduction level the trend of the line-shape-parameters was different as

discussed earlier. A similar trend was also noted for Alloy EP-823, as shown in Figure 4.16 (a, b and c).

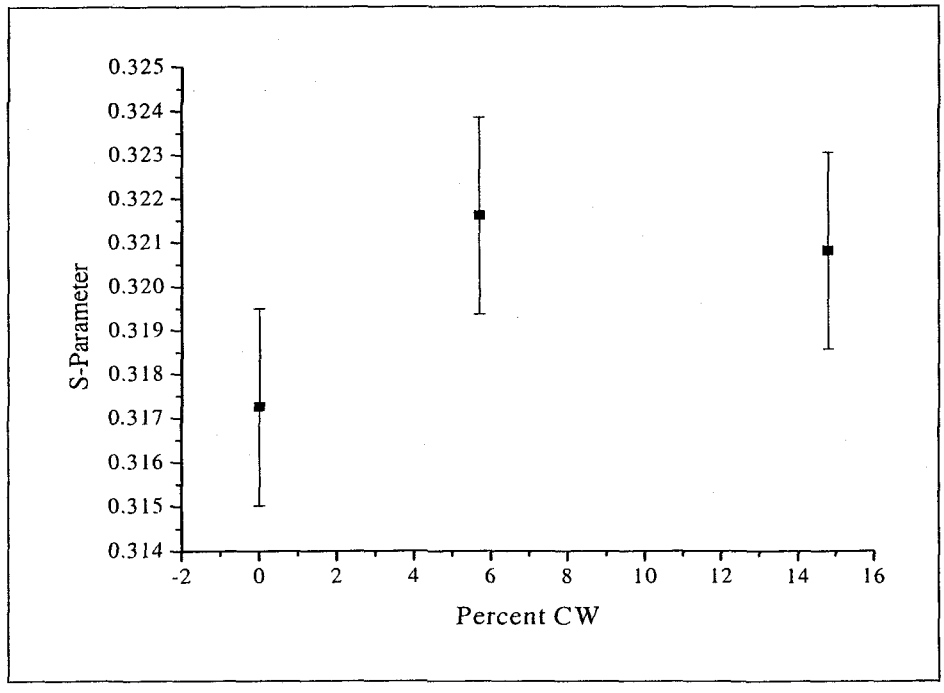

(a)

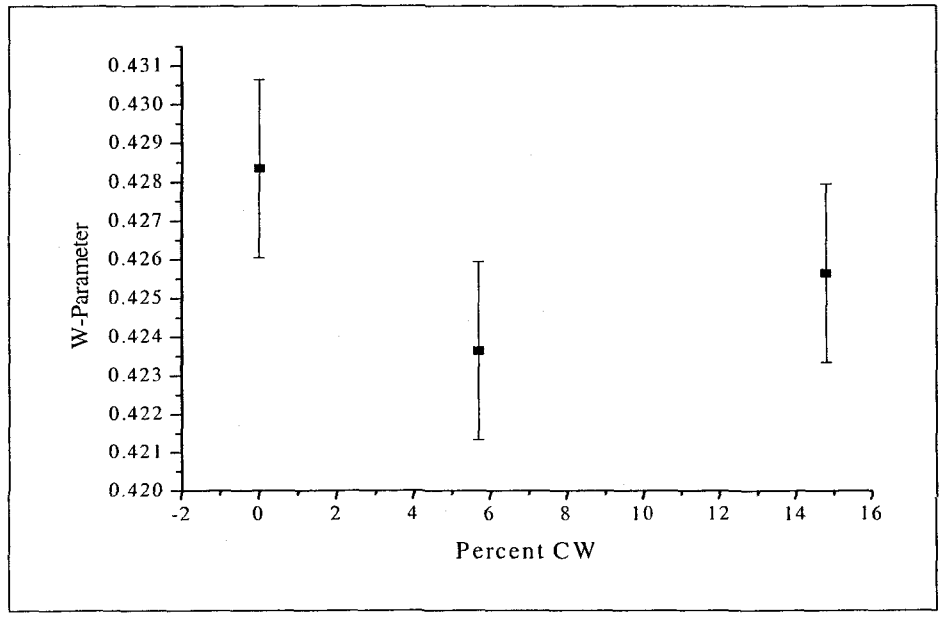

(b)

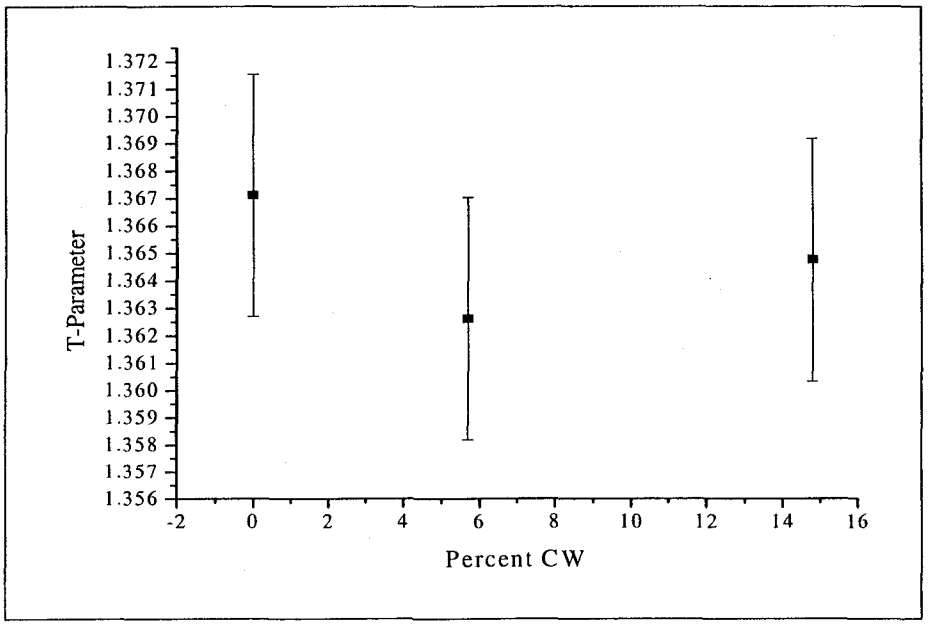

(c)

Figure 4.15 S, W and T –Parameter vs. Percent CW for Alloy HT-9 (Pair-production)

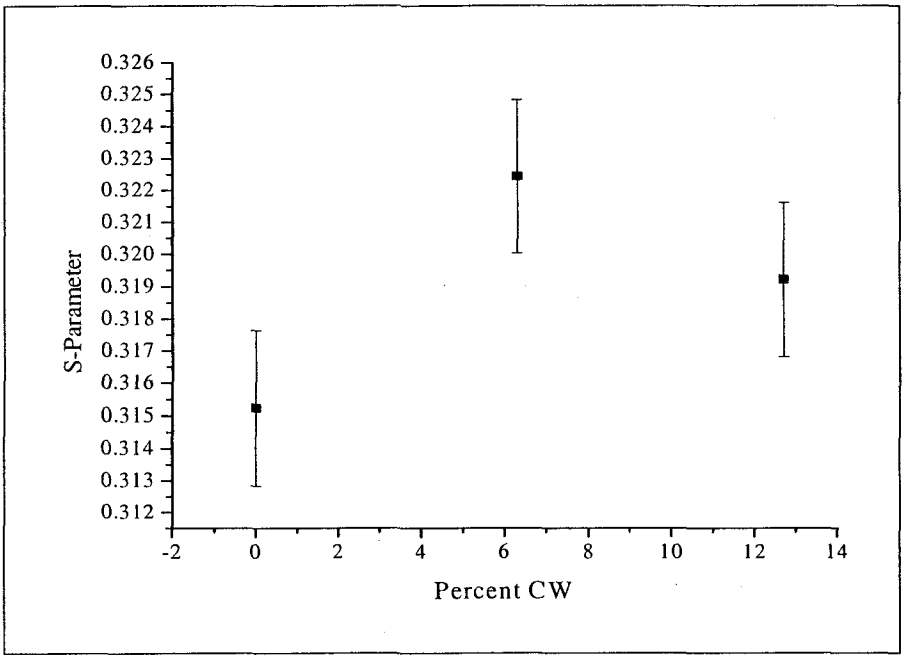

(a)

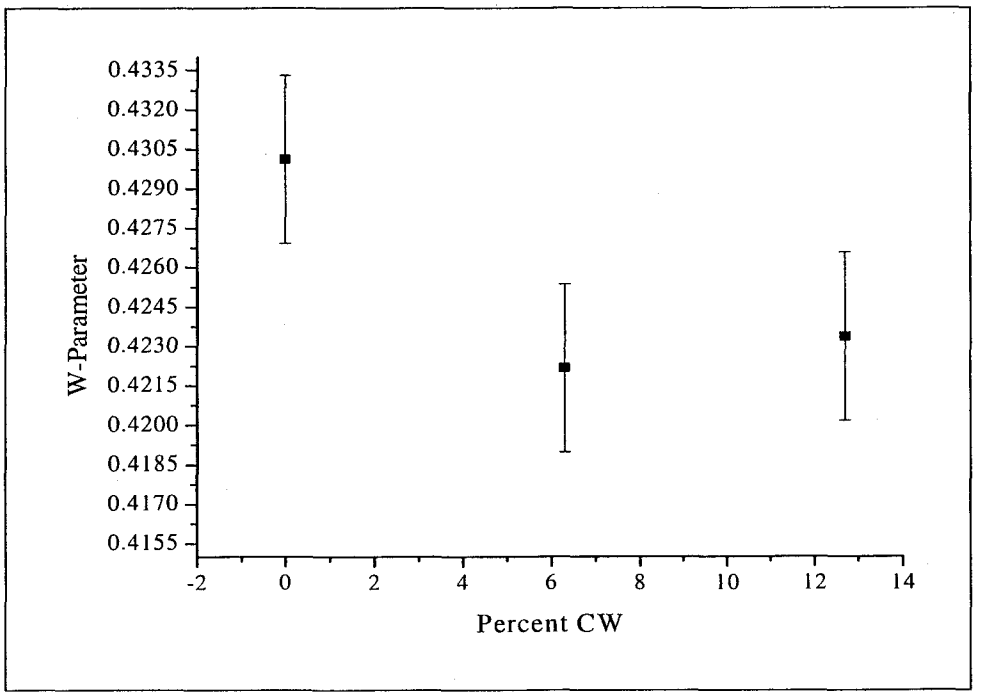

(b)

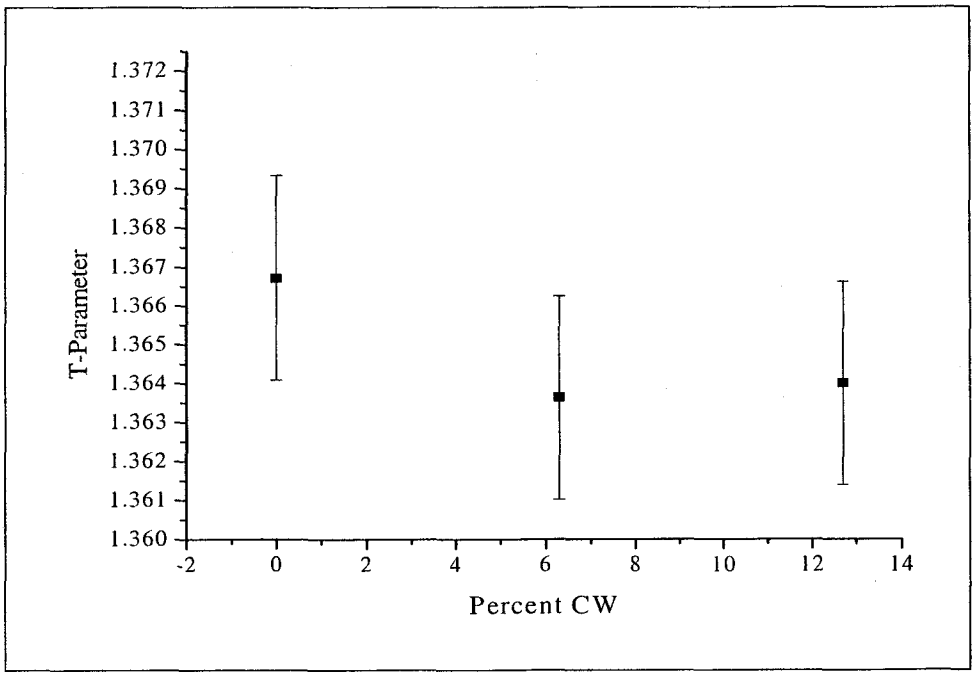

(C)

Figure 4.16 S, W and T-Parameter vs. Percent CW for Alloy EP-823 (Pair-Production)

4.3.4 Evaluation of Cylindrical Specimens by Pair-Production.

The results of residual stress characterization of plastically-deformed cylindrical specimens of Alloys HT-9 and EP-823 by the pair-production technique are shown in Figures 4.17 (a, b and c) and 4.18 (a, b and c) respectively. Similar relationships of S,W and T- Parameter to the applied stress was noted in these Figures.

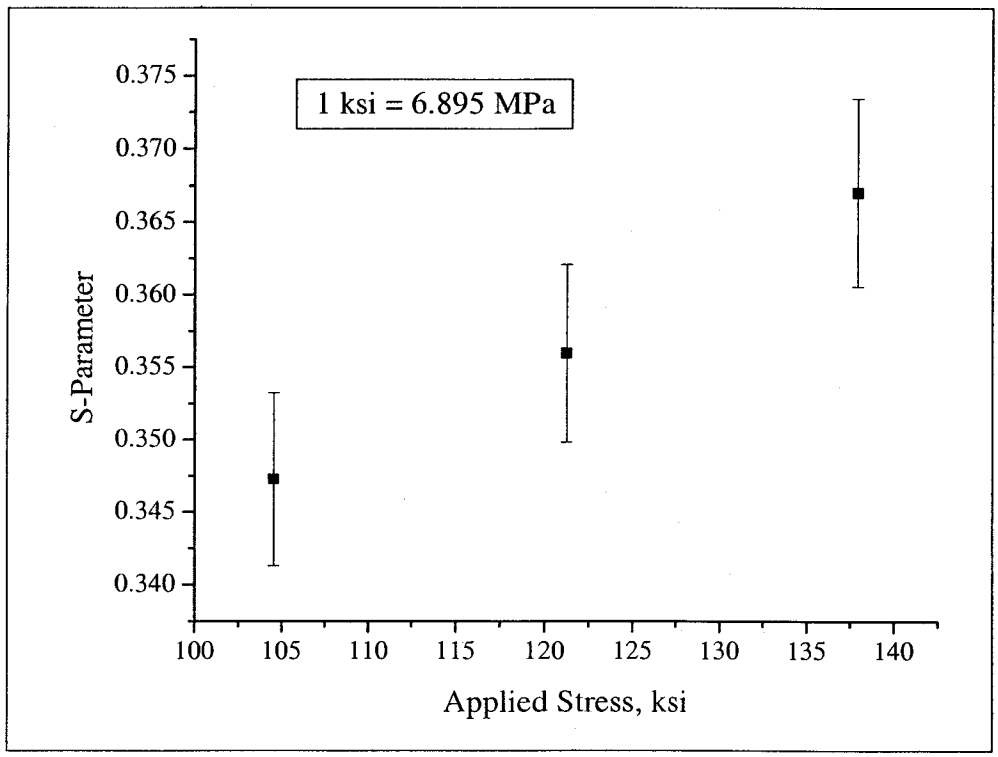

(a)

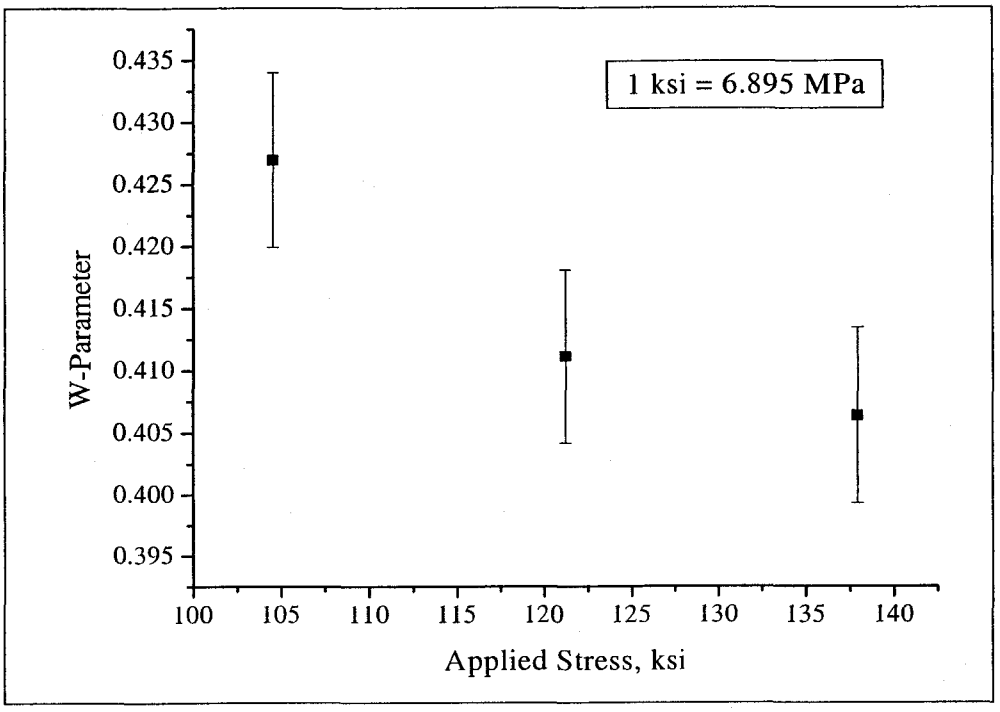

(b)

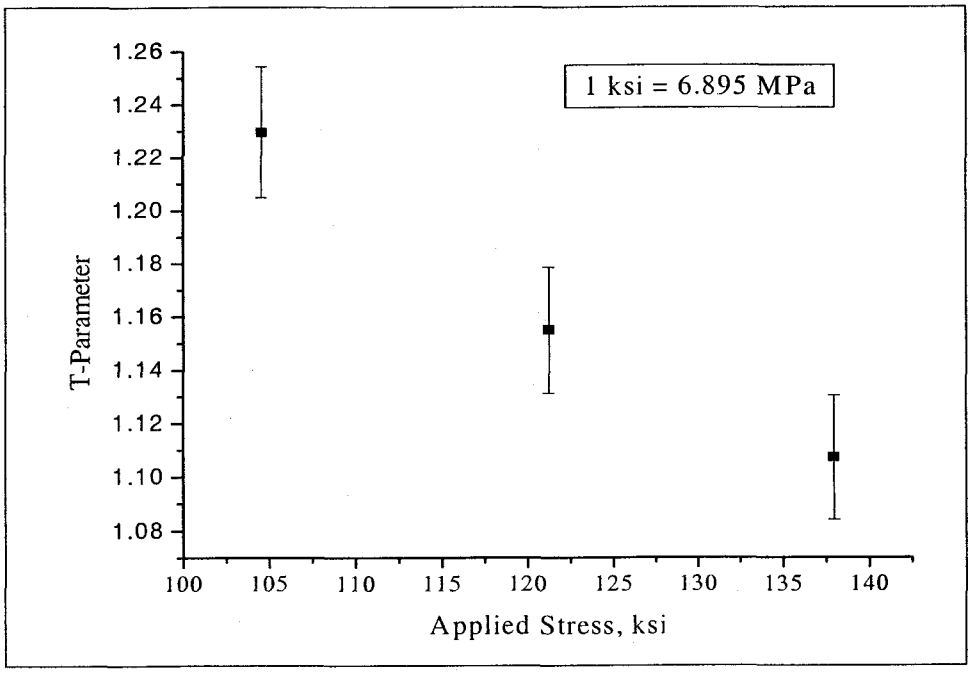

(c)

Figure 4.17 – S, W, and T-Parameter vs. Applied Stress for Alloy HT-9 (Pair-Production)

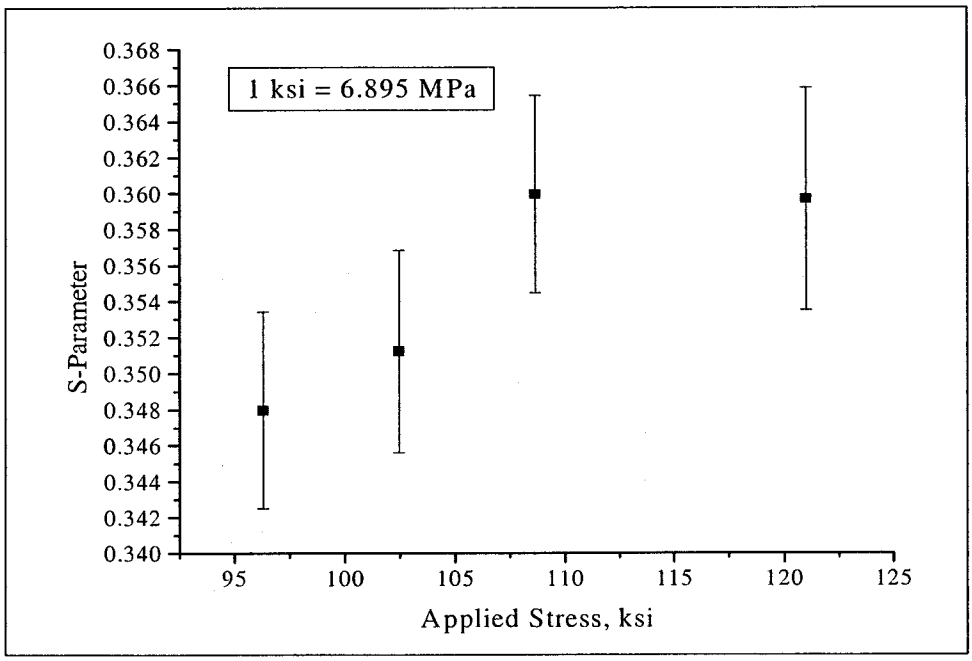

(a)

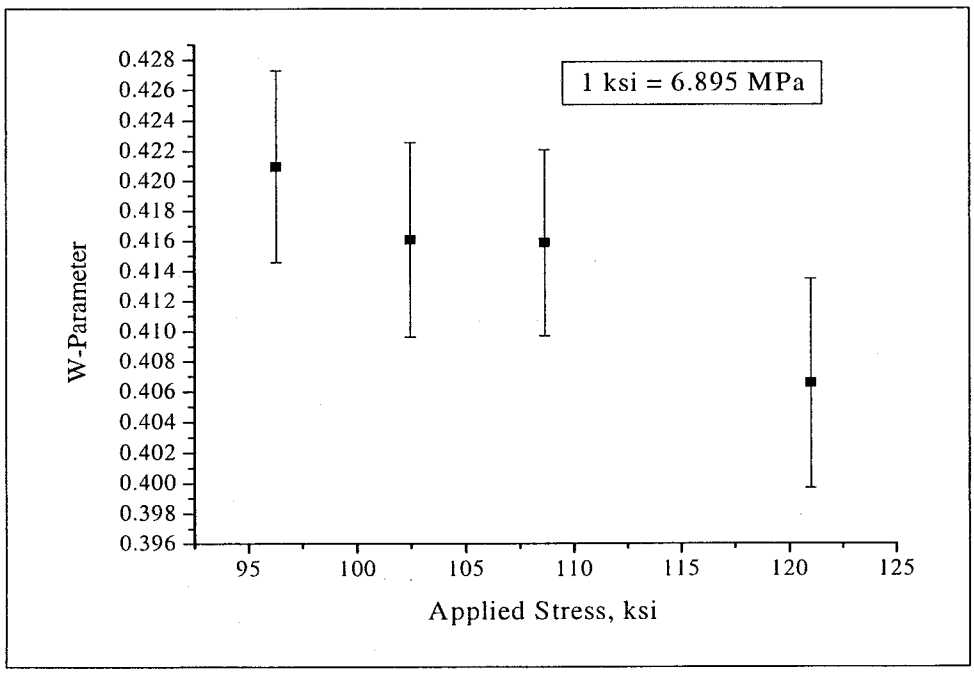

(b)

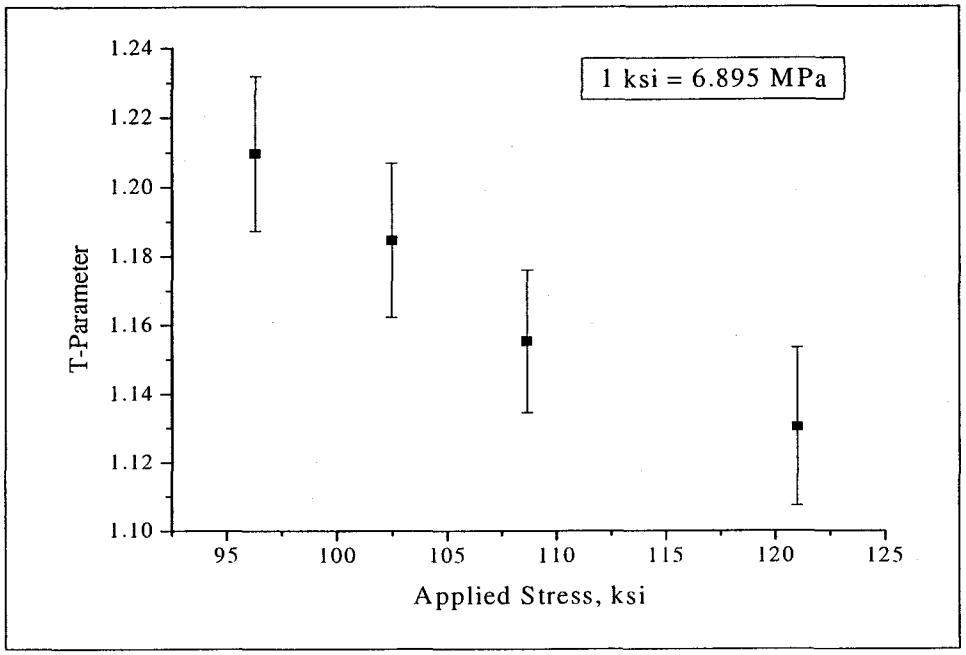

(c)

Figure 4.18 – S, W, and T-Parameter vs. Applied Stress for Alloy EP-823 (Pair-Production)

4.4 Comparison of Residual Stress by ND and PAS

As indicated earlier, the application of positron annihilation spectroscopy (PAS) was aimed at establishing this technique as a standard nondestructive tool of estimating the residual stress in cold-worked and plastically deformed structural materials since the neutron diffraction (ND) technique was capable of providing quantitative residual stress, attempts were made to compare the measured ND data to the estimated residual stress in plastically deformed cylindrical specimens in terms of S, W and T-parameters (pair-production) as a function of the applied tensile stress. A comparative analyses of the ND data and S,W and T-parameter versus the applied tensile stress is presented in

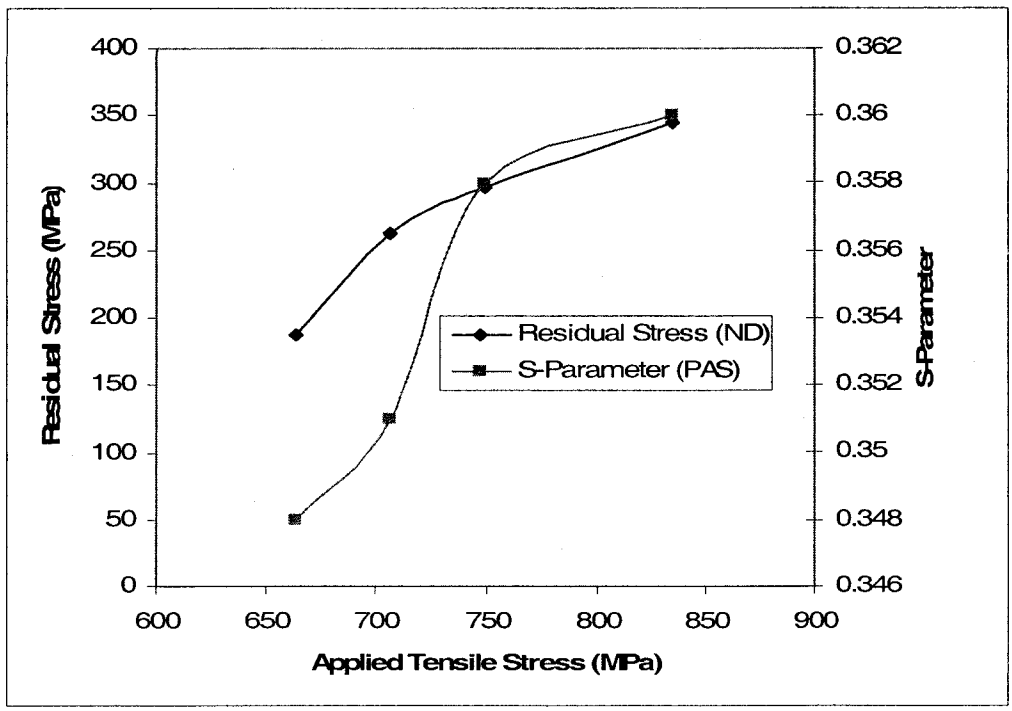

(a) ND Data vs. S-Parameter

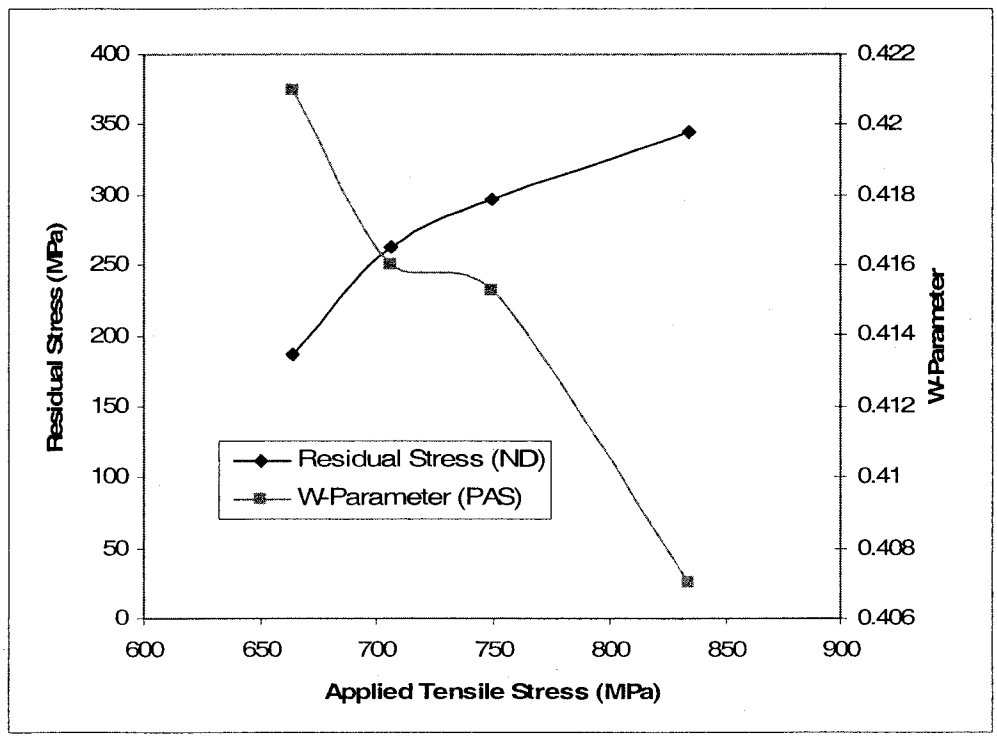

(b) ND Data vs. W-Parameter

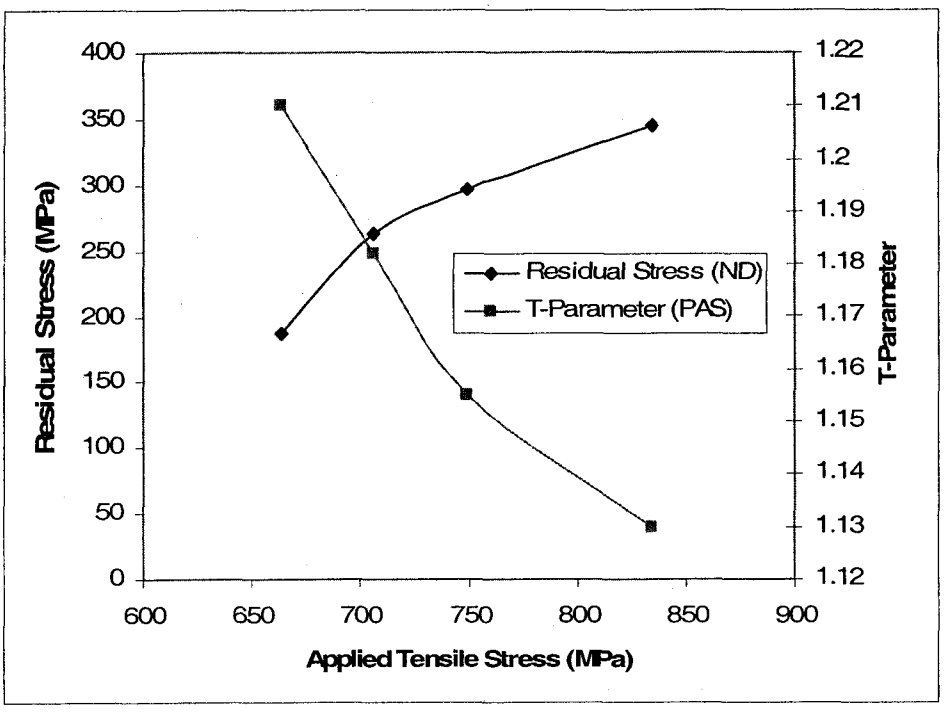

(c) ND Data vs. T-Parameter

Figure 4.19 Comparison of Residual stress by ND and PAS vs. Applied Stress on Alloy EP-823

Figure 4.19. An evaluation of these analyses indicated that there was an unique relationship of residual stress determined by ND technique to the PAS line-shape-parameters.

4.5 Characterization of Defects by TEM

It is well known that plastic-deformation of structural materials can lead to the generation of defects such as dislocations and voids. Therefore, significant efforts were made to characterize defects in plates of Alloy EP-823 subjected to reduction in thickness by 7 and 11%. For comparison purpose, a plate of EP-823 without any cold-reduction was also included for analysis of the nature and extent of defects by transmission electron

microscopy (TEM). The strain energy expended during plastic-deformation is usually stored in the metal lattice in the form of dislocations or other imperfections such as point defects. Thus, a strain-hardened metal such as Alloy EP-823 [42, 43] should have a higher strain energy in terms of dislocation density (ρ) compared to that of an unstrained material.

The TEM micrographs of Alloy EP-823 at different levels of cold-reduction are illustrated in Figures 4.20 through 4.22. An examination of Figure 4.20 indicates that the undeformed EP-823 plate was characterized by the presence of tempered martensitic laths and fine globular carbide precipitates. Even though, no attempts have been made in this investigation to characterize the nature of carbides, there are indications in the open literature [42-47] that this precipitates could be of the type M_7C_3, $M_{23}C_6$, M_3C and MC. It is also interesting to note that some residual dislocations were retained by the heat-treated Alloy EP-823 even without any cold-reduction that could have resulted from plastic-deformation prior to the heat-treatment operations.

The evaluation of the TEM micrographs corresponding to 7 and 11% cold-reduction, shown in Figures 4.21 and 4.22, respectively revealed the presence of enhanced dislocation clusters, as expected. It is interesting to note that the TEM micrograph, shown in Figure 4.21 was characterized by dislocations crossing one another at various locations within the metal lattice. A similar nature of dislocations was also noted for 11% cold-reduced Alloy EP-823, as illustrated in Figure 4.22. All three micrographs were utilized to calculate the density of dislocation (ρ) as a function of cold-reduction level. The average calculated values of ρ, corresponding to different cold-reduction levels determined by the line-intersection method discussed in the previous section are given in

the table 4.1. These results indicate that the magnitude of ρ was enhanced with increased cold-reduction level, as expected. The dislocation density, as reported by these investigators, was higher for martensitic Alloys tempered for shorter durations, thus resulting in higher residual stresses compared to that in materials tempered for longer durations.

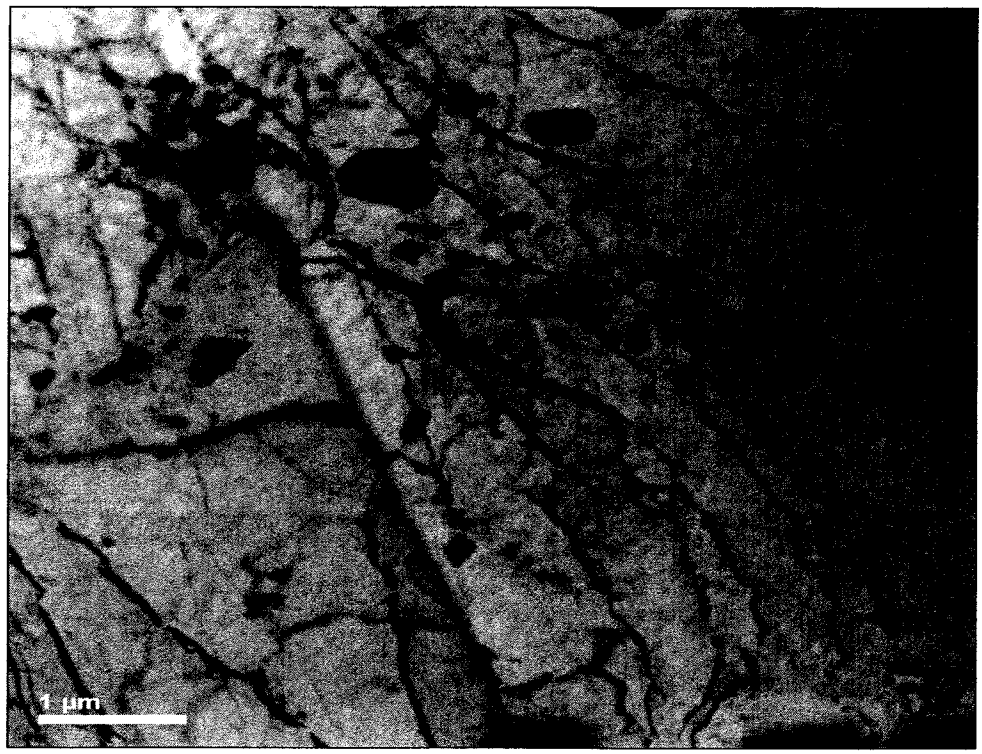

Figure 4.20 TEM Micrograph of Cold-Worked Specimen With No CR

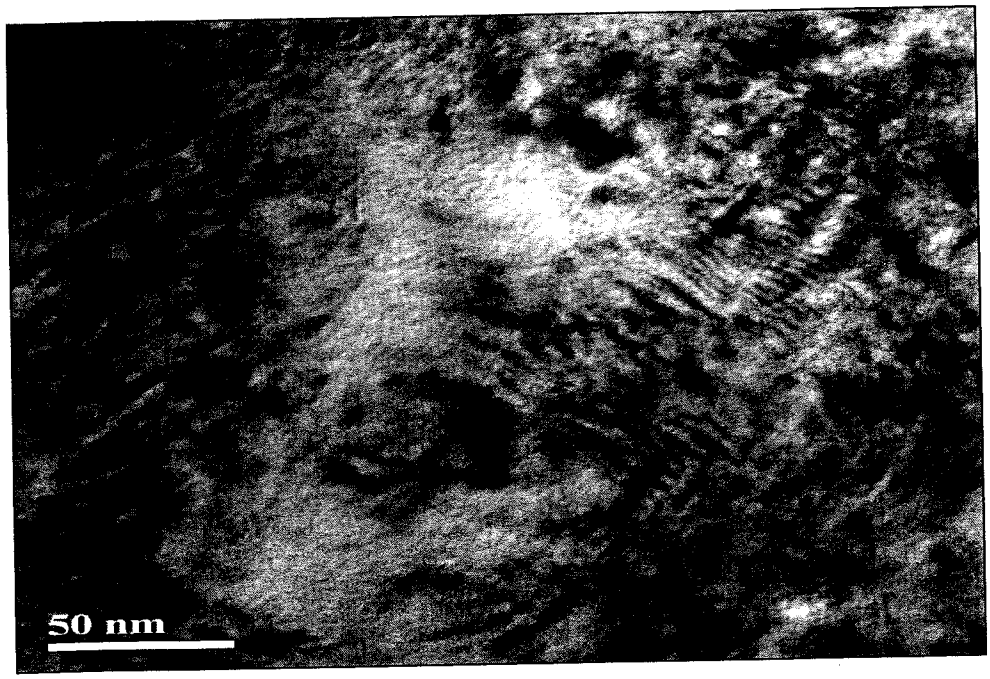

Figure 4.21 TEM Micrograph of 7.2 % CR Specimen

Figure 4.22 TEM Micrograph of 11.6% CR Specimen

Table 4.2 Dislocation Density of Alloy EP-823 at Different CR Levels

Percent cold reduction	Dislocation density, ρ (No./m^2)
0	2.645×10^{15}
7	9.834×10^{15}
11	6.157×10^{16}

4.6 Fractographic Evaluation by SEM

The extent and morphology of failure at the primary fracture surface of the cylindrical specimens used in calibration experiments were analyzed by scanning electron microscopy (SEM). The SEM micrographs of Alloy EP-823 and Alloy HT-9 are shown in Figures 4.22 and 4.23, respectively. An evaluation of these micrographs clearly revealed the presence of dimples, suggesting ductile failures in both materials.

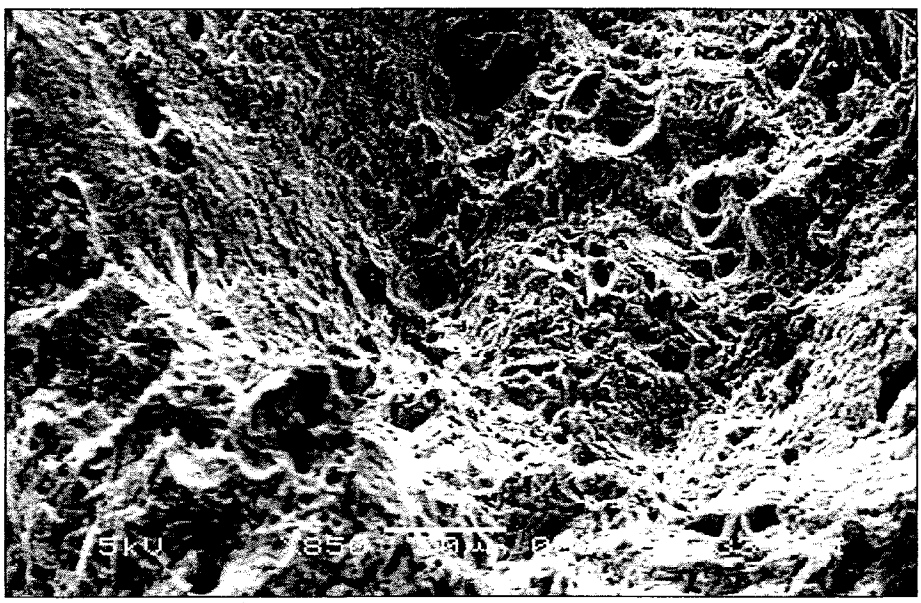

Figure 4.23 SEM Micrograph of Alloy HT-9, 850 X

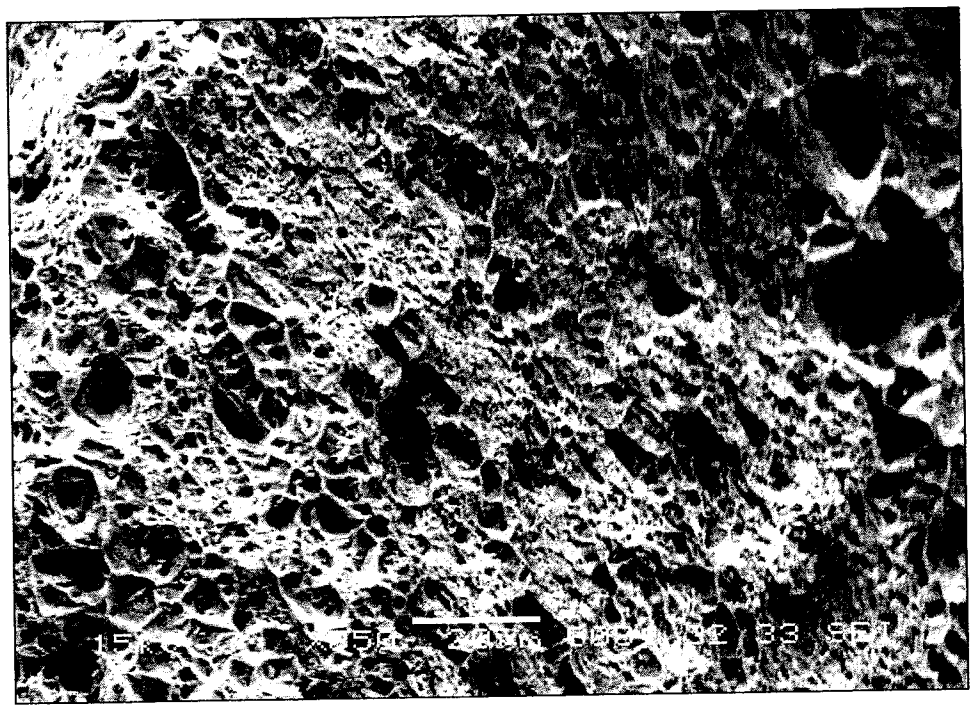

Figure 4.24 SEM Micrograph of Alloy EP-823, 850X

CHAPTER 5

DISCUSSION

Two martensitic materials, namely Alloys EP-823 and HT-9 were evaluated by the pair-production, activation and neutron-diffraction (ND) techniques to characterize residual stresses resulting from cold-reduction, plastic deformation and welding. A major emphasis has been made in this study on the ND technique, and subsequent comparisons have been made with data generated by the pair-production and activation techniques based on the classical positron annihilation spectroscopy (PAS).

The results of residual stress measurements by the ND technique on undeformed specimens indicate that insignificant tensile and compressive internal stresses were observed through out the thickness of both plate materials. These internal stresses could possibly be the results of prior forming operations imparted to the alloys, before thermal treatments with respect to the cold-reduced specimens, both alloys showed tensile residual stresses at the top and bottom surface of the plate. On the contrary compressive residual stresses were observed at some intermediate depth within the specimen thickness. These results clearly suggest that the extent of internal stress developed in the plate material will be maximum on both surface during cold-rolling operation used to provide the specific levels of reduction in thickness. Since both the activation and pair-production techniques can provide qualitative information on the resultant residual stress in cold-worked materials, evaluations of the S, W and T parameters were performed as a

function of the cold-reduction levels. The resultant data indicate that the S-parameter was gradually enhanced with the increased level of cold-reduction, indicating higher internal stresses. Conversely, the magnitudes of W and T Parameters were gradually reduced, once again showing higher internal stresses.

However, the maximum residual stresses were found at the highest level of cold-reduction and the S, W and T parameters showed the opposite trend at this reduction levels indicating decreased residual stresses. These data, in essence, verify that the S-parameter is directly proportional to the internal stresses while the other two PAS parameters are inversely proportional to the residual stress due to cold-reduction.

As discussed above, the pair-production and activation techniques can provide estimate levels of residual stresses in terms of the line-shape-parameters S, W and T. Therefore in order to achieve a quantitative evaluation of residual stress, cylindrical specimens plastically deformed by tensile loading at different levels, were subjected to residual stress characterization by the ND, pair-production and activation techniques. The evaluations of the activation and pair-production data involving cylindrical specimens indicate that, once again the S-Parameter was gradually enhanced at higher applied tensile stress levels. Similarly, the W and T parameters were gradually reduced with increased applied stress levels. Thus similar relation ships of S, W and T Parameters to the internal stress in both cold-worked and plastically cylindrical specimens can be established by both the activation and pair-production techniques. A similar phenomenon was also noted with cylindrical specimens, loaded at different plastic stress levels, evaluated by the ND technique, showing enhanced residual stresses at higher applied stress levels.

The characterization of residual stresses in welded specimens consisting of martensitic alloys on both sides, by the ND technique exhibited a benificial effect of post-weld-thermal-treatment (PWTT) in reducing the internal stresses. It is also interesting to note that the magnitude of residual stress was gradually reduced with distance away from the weld region. Once again these data are consistent with the basic understanding on welding in that the maximum stress due to welding is generated in the vicinity of the fusion line of a welded structure.

As to the micro-structure of both tested materials, fine-grained and fully-tempered martensitic microstructures were observed. The SEM study of the primary fracture surface of both alloys revealed dimpled microstructure, typical of ductile failures. The characterization of defects in cold-worked Alloy EP-823 by TEM demonstrated that the dislocation density was increased with increasing cold-reduction levels.

CHAPTER 6

SUMMARY AND CONCLUSIONS

Martensitic Alloys EP-823 and HT-9, subjected to cold-reduction, plastic-deformation and welding, were characterized for residual stress evaluations by ND, pair-production and activation techniques. Since the pair-production and activation techniques can provide qualitative information, determination of calibration curves was performed by using all three techniques. The nature and extent of defects due to cold-reduction of Alloy EP-823 were analyzed by transmission electron microscopy (TEM). The morphology of failure of the cylindrical specimens used in calibration study was also analyzed by scanning electron microscopy (SEM). The significant conclusions derived from this investigation are given below.

- The residual stresses at the top and bottom surfaces of the cold-worked specimens determined from the ND measurements, were tensile in nature
- A combination of insignificant tensile and compressive internal stresses was observed in specimens without any cold-reduction, possibly due to the effect of prior forming operations.
- The magnitude of residual stress in plastically deformed cylindrical specimen was enhanced with increasing applied stress ranging between the yield stress and the ultimate tensile stress

- The extent of residual stress in the welded specimens was reduced at locations away from the fusion-line, as expected. PWTT was beneficial to reduce these internal stresses
- The residual stress estimated by the S-parameter was gradually enhanced at higher levels of cold-reduction. At the highest level of cold-reduction the S-parameter was decreased indicating reduced residual stress. Similarly, the magnitude of internal stress in the cylindrical specimens was enhanced at higher applied stress level, showing enhanced S-parameter value.
- The W and T- parameters were gradually reduced with increased cold-reduction and applied stress levels, suggesting that these two parameters are inversely proportional to the resultant internal stresses. However, at highest cold-reduction level it increased showing the increased residual stress value the reason for which was discussed earlier in chapter 4 of this thesis.
- The dislocation density was increased with increased levels of cold-reduction, as determined by TEM.
- The failure experienced by the cylindrical specimens at their primary fracture surfaces was characterized by dimples, indicating ductile failures.

CHAPTER 7

SUGGESTED FUTURE WORK

The following additional work for future evaluations are suggested

- Evaluation of effect of PWTT on residual stress by the PAS technique.
- Characterization of defects in welded specimens by TEM

CHAPTER 7

SUGGESTED FUTURE WORK

The following additional work for future evaluations are suggested

- Evaluation of effect of PWTT on residual stress by the PAS technique.
- Characterization of defects in welded specimens by TEM

APPENDIX A

TEM Micrographs of Alloy EP-823 subjected to different levels of cold-reduction

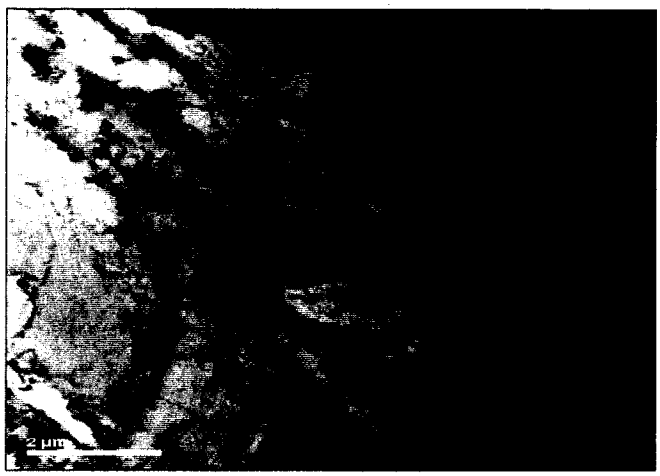

(a)

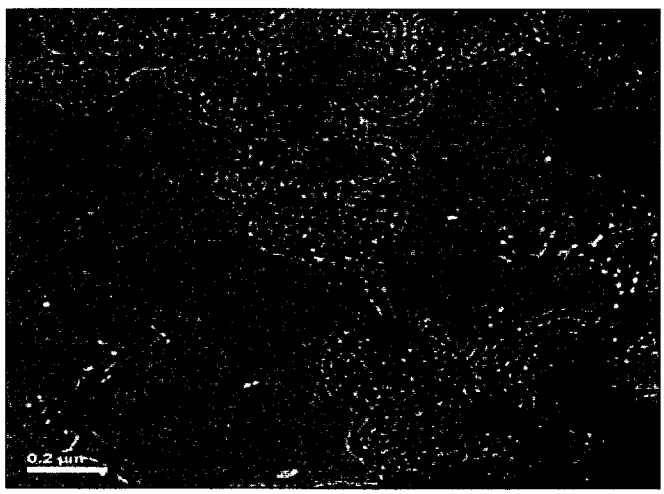

(b)

TEM Micrographs of Alloy EP-823 With No Cold-reduction

(a)

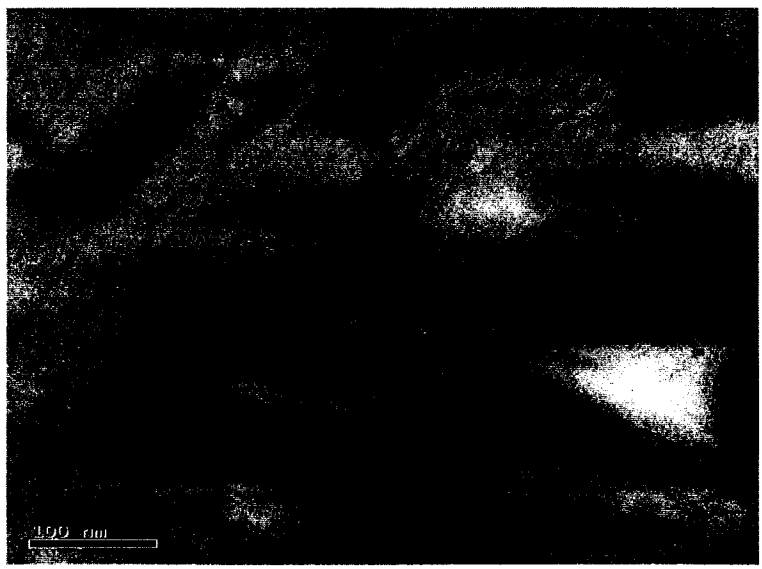

(b)

TEM Micrographs of Alloy EP-823 With 7.2% Cold-reduction

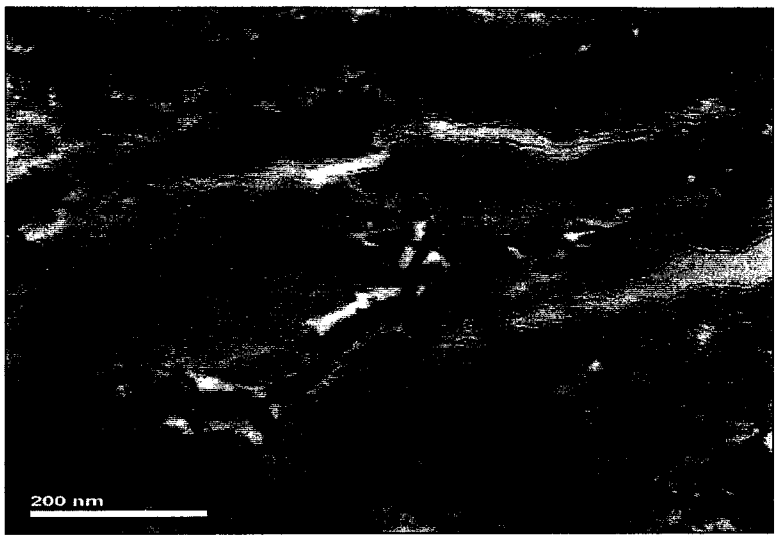

(a)

(b)

TEM Micrographs of Alloy EP-823 With 11.6% Cold-reduction

APPENDIX B

SEM MICROGRAPHS

SEM Micrograph of Alloy EP-823, 35 X

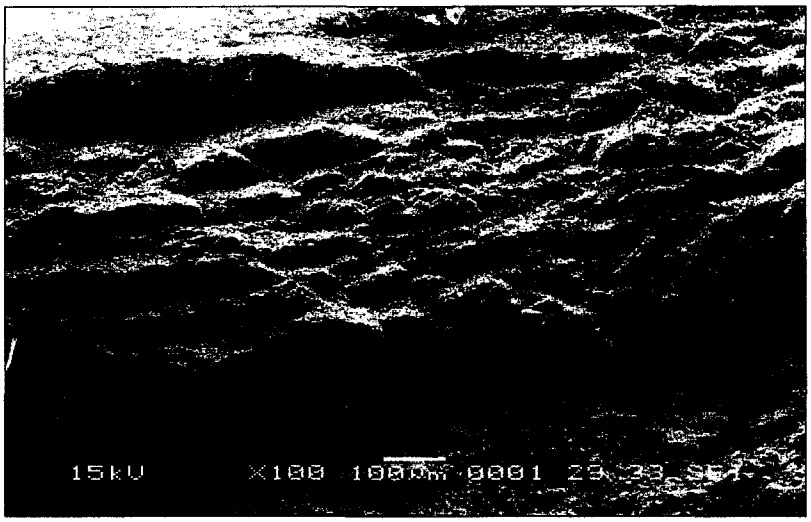

SEM Micrograph of Alloy EP-823, 100 X

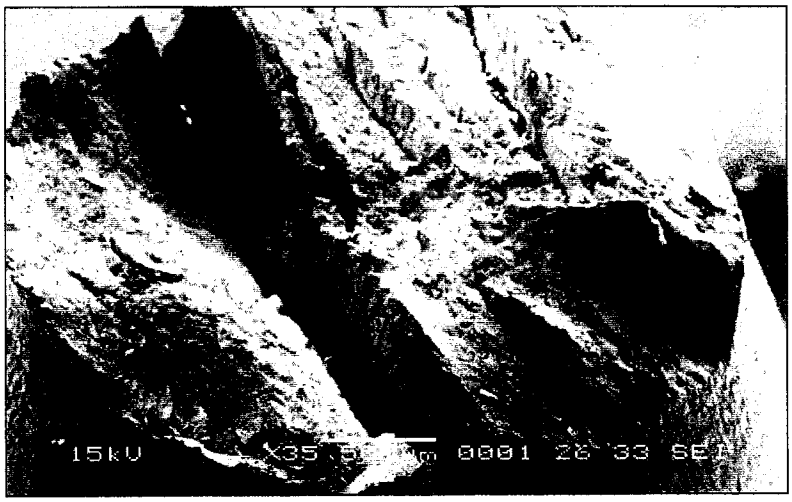

SEM Micrograph of Alloy HT-9, 35X

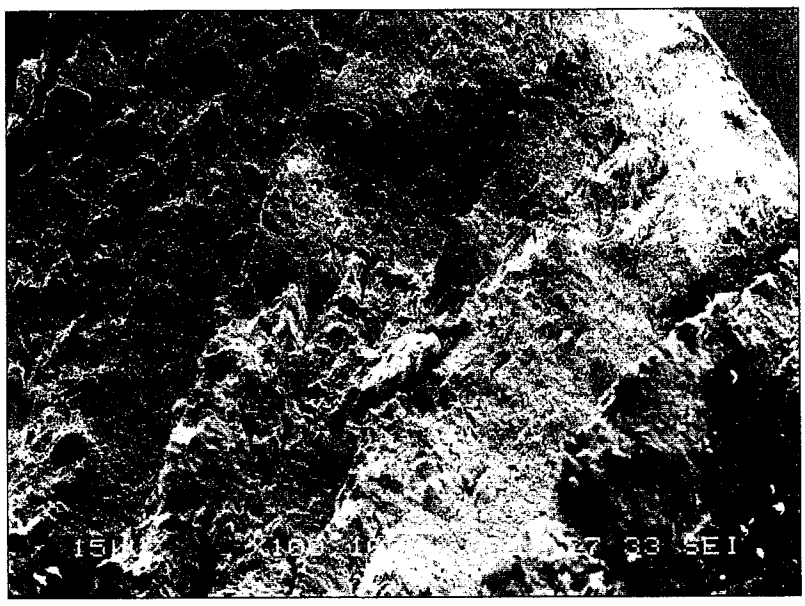

SEM Micrograph of Alloy HT-9, 100X

BIBLIOGRAPHY

1. Doering, Thomas W. Pasupathi, Waste package and material testing for the proposed Yucca mountain high-level waste repository, JNMM, 2002, 31-35.

2. Gonzalez, E. Embid, M. Transmutation of radioactive wastes, Nuclear Espana, 2003, 230 30-34.

3. http://www.jaeri.go.jp/english/press/990528/fig07.html

4. Kandil, F.A., Lord J.D., Fry, A.T., Grant, A.V., A Review of Residual Stress Measurement Methods- A guide to Technique selection, NPL Report MATC (A) 04, National Physical laboratory, February 2001

5. A. K. Roy, A. K.; Venkatesh, A.; Marthandam, V.; Dronavalli, S. B.; Wells, Douglas; Rogge, Ronald. Residual stress characterization in structural materials by destructive and nondestructive techniques. Journal of Materials Engineering and Performance, 2005, pp 203-211.

6. Mechanical Properties of Stainless Steel, Outokumpu Stainless Website (http://www.outokumpu.com/pages/page___5761.aspx)

7. H.E Boyer (Ed.), Metals Handbook, vol. 10, American Society for Metals, Metals Park, Ohio, 1975, pp. 217-218.

8. S .I. Porollo, Yu. V. Konobeev, and A. M. Dvoriashin (State Scientific Center of Russian Federation, (The Institute of Physics and Power Engineering, 249020 Obninsk, Russia) N. I. Budylkin, E. G. Mironova, M. V. Leontyeva-Smirnova, and A. G. Loltukhovsky (State Scientific Center of Russian Federation, A. A. Boinchvar All-Russia Research Institute of Inorganic Materials (VNIINM), Moscow, Russia) and F. A. Garner (Pacific Northwest National Laboratory) "Irradiation Creep and Mechanical Properties of two ferritic/martensitic steels irradiated in the BN-350 fast reactor"

9. Zihni Ozturk, Monroe S. Wechsler, Effects of High Energy Protons on the Mechanical Properties of Fe-2.25Cr-1Mo and Fe-12Cr-1Mo Steels, Transactions of the. Journal of Engineering and Environmental Science, 1998, pp.197- 222

10. Elliott, C., Lucas, G.E., Maiti, R., Odette, G.R., Microstructure of HT-9 as a function of Heat Treatment, J.Nucl.Mater., 141-143, 1986, p794

11. A.J. Griffiths and A.TurnbullL: Proc. Conf on Structural Materials in Marine Environments, London, UK, May 1994, the Institute of Materials, 324-329.

12. Zihni Ozturk, Monroe S. Wechsler, Effects of High Energy Protons on the Mechanical Properties of Fe-2.25Cr-1Mo and Fe-12Cr-1Mo Steels, Transactions of the Journal of Engineering and Environmental Science, 22 , pp. 197-202(1998)

13. ASTM Designation: E 8-89b, Standard Test Methods of Tension Testing of Metallic Materials

14. http://www.key-to-steel.com/Articles/Art97.htm

15. Anand Venkatesh, M.S Thesis, Comparative Analyses of Residual stresses in Target Subsystem Materials

16. Subhra Bandyopadhyay, Characterization of Defects by Transmission Electron Microscopy

17. A. K.Roy, S. Bandyopadhyay, S. B. Suresh, D. Maitra, P. Kumar, D. Wells, L. Ma, Relationship of Residual stress to Dislocation Density in Cold-Worked Martensitic Alloy (in print)

18. http://en.wikipedia.org/wiki/Electron-positron_annihilation

19. F.A. Selim, D.P. Wells, J.F. Harmon, J. Kwofie, R. Spaulding, G. Erickson, and T.Roney., Nucl. Instrum. Methods Phys. Res. A, Vol. 495 No.2, 2002, pp. 154-160

20. A. K. Roy, A.Venkatesh, V. Marthandam, S.B.Dronavalli, Douglas Wells, and Ronald Rogge, ASM International, November 4 2004, Residual Stress Characterization in Structural Materials by Destructive and Nondestructive Techniques

21. P. Asoka-Kumar, K.G. Lynn, and D.O. Welch, J. Appl. Phys., Vol. 76, No.9, 1994, pp. 4935-4982

22. P. Hautojarvi and A. Vehanen, Positrons in Solids, Springer-Verlag, New York, 1979, pp. 1-20

23. A. W. Hunt, R. Spaulding, J. Urban-Klaehn, J. F. Harmon, D. P. Wells, Nucl. Instr. & Meth. B., (in print), Oct 2005

24. I. K. MacKenzie, T. L. Khoo, A. B. McDonald, B. T. A. McKee., Phys. Rev. Lett, Vol. 19, 1967, pp. 946

25. B. T. A. McKee, S. Saimoto, A. T. Stewart and M. J. Scott, Canadian Journal of Physics, Vol. 52, 1974, pp. 759

26. S. Saimoto, B. T. A. McKee, A. T. Stewart, Phys. Status Solids., A21, 1974, pp. 623

27. K. G. Lynn, R. Ure, J. G. Byrne, Acta Metall., Vol. 22, 1974, pp. 1075

28. A. Lodini, The recent development of neutronic techniques for determination of residual stresses.

29. G.A. Webster, R.C. Wimpory, Non-destructive measurement for residual stress by neutron diffraction, Journal of Materials Processing Technology,2001, pp.395-399

30. T.Lorentez, J.B. Ibso, Neutron diffraction measurements of residual strains in offshore welds, Materials Science and Engineering 1995, pp. 209-214.

31. T.M. Holden, The Determination of Macrostresses and Microstresses by Neutron Diffraction, Materials Research Society Symposia Proceedings, Volume 376, pp.385-390

32. Man Jin Park, Hee Nam Yag, DongY.Jang, Jong Sung Kim, Tae Eun Jin, Residual Stress Measurement On Welded Specimen by Neutron Diffraction, Journal of Materials Processing Technology 155-156 (2004), pp. 1171-1177

33. http://neutron.nrc-cnrc.gc.ca/l3gen.html

34. M.S. Mechanical Engineering, Venkata Potluri, "Effect of Heat Treatment on Deformation and Corrosion Behavior of Type 422 Stainless Steel" Aug. 2004

35. M.S. Mechanical Engineering, Srinivasa Kukatla, "Corrosion and High-Temperature Deformation Characteristics of a Target Structural Material for Transmutation Applications" Dec 2003

36. Hirsch P, Howie A, Nicholson R, Pashley DW, Whelan MJ. Electron microscopy of thin crystals. Malabar: Krieger Publishing company, 1977

37. Loretto MH. Electron beam analysis of materials. London: Chapman and Hall, 1994

38. J. Pesicka, R. Kuzel, A. Dronhofer, G. Eggeler, Acta Materialia, Vol. 51, 2003, pp. 4847-4862

39. R. F. Egerton, Electron Energy Loss Spectroscopy in the Electron Microscope, Plenum Press, 1986, pp. 291-352

40. A.K. Roy, S.R. Kukatla, B. Yarlagadda, V.N. Potluri, M. Lewis, M. Jones, and B.J. O'Toole, JMEPEG, Vol. 14, No.2, April 2005, pp. 212-218

41. S. Gündüz, Ironmaking and Steelmaking, Vol. 29, No.5, 2002, pp. 341-346

42. N. Mebarki, D. Delagnes , P. Lamesle, F. Delmas, C. Levaillant, Materials Science

and Engineering A, Vol 87, 2004, pp. 171-175

43. N. Mebarki, Ph.D. Thesis, Ecole Nationale Supérieure des Mines de Paris, February 2003.

44. J. Gubicza, J. Szépvölgyi, I. Mohai, L. Zsoldos, T. Ungár, Materials Science Engineering. A, Vol. 280, 2000, pp. 263.

45. T. Ungár, S. Ott, P.G. Sanders, A. Borbély, J.R. Weertman, Acta Mater., Vol. 46, 1998, pp. 3693.

46. T. Ungár, J. Gubicza, G. Ribárik, A. Borbély, J. Appl. Crystallogr. Vol 34, 2001, pp. 298.

47. N. Mebarki, P. Lamesle, D. Delagnes, F. Delmas, C. Levaillant, in: J. Bergström, G. Fredriksson, M. Johansson, O. Kotik, F. Thuvander (Eds.), Proceedings of the 6th International Tooling Conference, The Use of Tool Steels: Experience and Research, Karlstad University, Sweden, 10–13 September 2002, pp. 617–632.

VITA

Graduate College
University of Nevada, Las Vegas

Silpa Budugur Suresh

Address:
969 East Flamingo Road, Apt # 167
Las Vegas, NV89119

Degrees:
Bachelor of Science, Mechanical Engineering, June 2003
Sri Venkateswara University

Special Honors and Awards:

- Student Member, The American Society of Mechanical Engineers (ASME)
- Student Member, The American Nuclear Society (ANS)

Publications:

- Subhra Bandyopadhyay, Silpa Budugur Suresh, "Calibration Curves for Stress-Strain Measurements by Positron Annihilation Spectroscopy" American Nuclear Society (ANS) Student Conference, April 14-16, Columbus, OH

- A.K.Roy, Silpa Budugur Suresh et al;, "Residual Stress Measurements in Structural Materials by Nondestructive technique" SAMPE 2005 Symposium and Exhibition (50^{th} ISSE), May 3-5, 2005, Long Beach, CA

- Subhra Bandyopadhyay, Silpa Budugur Suresh, "Residual Stress Measurements in Martensitic Stainless Steel" accepted for presentation at ASME Pressure Vessels & Piping Division Student Conference, July 17-21, 2005

- A.K.Roy, Silpa Budugur Suresh et al; "Characterization of Residual stresses in Structural Materials for Nuclear Applications" accepted for presentation at ASME Pressure Vessels & Piping Division Conference, July 17-21, 2005